UPPSALA
UNIVERSITET

Digital Comprehensive Summaries of Uppsala Dissertations from the Faculty of Science and Technology 1453

Electron-scale physics in space plasma

Thin boundaries and magnetic reconnection

CECILIA NORGREN

ACTA
UNIVERSITATIS
UPSALIENSIS
UPPSALA
2016

ISSN 1651-6214
ISBN 978-91-554-9755-2
urn:nbn:se:uu:diva-307955

Dissertation presented at Uppsala University to be publicly examined in Polhemsalen, Ångström Laboratory, Lägerhyddsvägen 1, Uppsala, Friday, 20 January 2017 at 10:00 for the degree of Doctor of Philosophy. The examination will be conducted in English. Faculty examiner: Dr/Lecturer Jonathan Eastwood.

Abstract

Norgren, C. 2016. Electron-scale physics in space plasma. Thin boundaries and magnetic reconnection. *Digital Comprehensive Summaries of Uppsala Dissertations from the Faculty of Science and Technology* 1453. 68 pp. Uppsala: Acta Universitatis Upsaliensis. ISBN 978-91-554-9755-2.

Most of the observable Universe consists of plasma, a kind of ionized gas that interacts with electric and magnetic fields. Large volumes of space are filled with relatively uniform plasmas that convect with the magnetic field. This is the case for the solar wind, and large parts of planetary magnetospheres, the volumes around the magnetized planets that are dominated by the planet's internal magnetic field. Large plasma volumes in space are often separated by thin extended boundaries. Many small-scale processes in these boundaries mediate large volumes of plasma and energy between the adjacent regions, and can lead to global changes in the magnetic field topology. To understand how large-scale plasma regions are created, maintained, and how they can mix, it is important understand how the processes in the thin boundaries separating them work.

A process in these thin boundaries that may result in large scale changes in magnetic field topology is magnetic reconnection. Magnetic reconnection is a fundamental process that transfers energy from the magnetic field to particles, and occurs both in laboratory and astrophysical plasmas. It is a multi-scale process involving both ions and electrons, but is only partly understood

Space above the Earth's ionosphere is essentially collisionless, meaning that information, energy, and mass transfer have to be mediated through means other than collisions. In a plasma, this can happen through interactions between particles and electrostatic and electromagnetic waves. Instabilities that excites waves can therefore play a crucial role in the energy transfer between fields and particles, and different particle populations, for example between ions and electrons.

In this thesis we have used data from ESA's four Cluster and NASA's four Magnetospheric Multiscale (MMS) satellites to study small-scale – the scale where details of the electron motion becomes important – processes in thin boundaries around Earth. With Cluster, we have made detailed measurements of lower-hybrid waves and electrostatic solitary waves to better understand what role these waves can play in collisionless energy transfer. Here, the use of at least two satellites was crucial to estimate the phase speed of the waves, and associated wavelength, as well as electrostatic potential of the waves. With MMS, we have studied the electron dynamics within thin boundaries undergoing magnetic reconnection, and found that the current is often carried by non-gyrotropic parts of the electron distribution. The non-gyrotropy was caused by finite gyroradius effects due to sharp gradients in the magnetic field and plasma density and temperature. Here, the use of four satellites was crucial to deduce the spatial structure and thickness of the boundaries. Before the MMS mission, these observations of electron dynamics have never been possible in space, due to instrumental limitations of previous missions. All these findings have led to better understanding of both our near-space environment and plasma physics in general.

Cecilia Norgren, Department of Physics and Astronomy, Box 516, Uppsala University, SE-751 20 Uppsala, Sweden. Swedish Institute of Space Physics, Uppsala Division, Box 537, Uppsala University, SE-75121 Uppsala, Sweden.

ISSN 1651-6214
ISBN 978-91-554-9755-2
urn:nbn:se:uu:diva-307955 (http://urn.kb.se/resolve?urn=urn:nbn:se:uu:diva-307955)

Till pappa,
som nog inte bryr sig om rymdfysik[1]*,*
men bryr sig om mig

[1] Jag har nog aldrig frågat...

List of papers

This thesis is based on the following papers, which are referred to in the text by their Roman numerals.

I Norgren, C., A. Vaivads, Y. V. Khotyaintsev, and M. Andre (2012), Lower hybrid drift waves: Space observations, Phys. Rev. Lett., 109, 55001, doi:10.1103/PhysRevLett.109.055001.

II Norgren, C., M. André, A. Vaivads, and Y. V. Khotyaintsev (2015), Slow electron phase space holes: Magnetotail observations, Geophys. Res. Lett., 42, doi:10.1002/2015GL063218.

III Norgren, C., M. André, D. B. Graham, Yu. V. Khotyaintsev, and A. Vaivads (2015), Slow electron holes in multicomponent plasmas, Geophys. Res. Lett., 42, doi:10.1002/2015GL065390.

IV Norgren, C., et al. (2016), Finite gyroradius effects in the electron outflow of asymmetric magnetic reconnection, Geophys. Res. Lett., 43, doi:10.1002/2016GL069205.

V Norgren, C., et al., Observation of high-shear bifurcated electron-scale current sheet at the magnetopause, Manuscript in preparation.

Contents

1. Introduction

The word space encompasses numerous imaginable and unimaginable things. Some might think of extraterrestrial life, while others think of the burning infernos that are stars. Some might think of the birth of the Universe, or how to use worm holes to effectively travel faster than light. Others think of the moons of Saturn, how the Earth interacts with the Sun, or how the aurorae is created. Some of these are far away phenomena and can only be studied on paper or through a telescope, while some are close enough for us to probe directly with ingeniously designed spacecraft.

Today we know that the major part of the observable universe is not made out of solids, nor liquids, nor gases. Everything made up of these states of matter, like the larger part of the Earth for example, is in fact floating around in a vast ocean of something else, namely *plasma* [22]. A plasma is a type of ionized gas, formed or sustained as electrons is removed from or adhered to neutral atoms through collisions with other atoms, molecules or high energy electromagnetic waves. Since a plasma is made up of negatively charged electrons and positively or negatively [24] charged ions [or positrons], it is subject to electromagnetic forces. Due to the nature of the electric (Coulomb's) force a plasma has to be *quasineutral* – having net zero charge. Any local region subject to charge imbalance will attract particles of the opposite charge until the charge is shielded away. Since the electrons due to their lower mass are more mobile than the ions, they typically do the shielding. If the velocity distribution of the electron population can be described by a Maxwellian distribution, the resulting potential due to a perturbing point-like charge is given by [22]:

$$\phi = \phi_0 e^{-r/\lambda_D}, \quad \text{where} \quad \lambda_{De} = \sqrt{\frac{e^2 n_\infty}{\varepsilon_0 k_B T_e}} \tag{1.1}$$

is known as the *Debye length*, ϕ_0 is the potential of the perturbing charge, n_∞ is the density far away from the charge, T_e is the electron temperature, r is the distance from the charge, e is the elementary charge, ε_0 is the permittivity of free space, and k_B is the Boltzmann constant. The direct effect of the charge is thus important only on scales comparable and inferior to the Debye length. Thus, for a plasma to be charge neutral, the typical length scale of the plasma, L, needs to be much larger than the Debye length, $\lambda_D \ll L$. Given the right conditions however, the initial perturbation due to the perturbing charge can propagate long distances via the combined effects of other particles, referred

to as collective behaviour. For the Debye shielding to be effective, and for the collective behaviour to apply, there need to be enough particles in the so called Debye sphere: $N_D = 4\pi\lambda_D^3/3 \gg 1$ [22].

Sometimes the electrons adhere to dust grains, forming negative particles that act as massive negative ions [58]. Generally, a plasma is only partially ionized, and the degree of ionization depends on the relative rates of ionization and recombination. When the degree of ionization is sufficiently low, such that the gas is dominated by hydrodynamic forces due to collision between neutral and charged particles, it is not considered a plasma. Often however, a partial ionization as low as 0.1 % is enough for the gas to behave as a plasma [22].

The term plasma was coined in 1928 by Irving Langmuir, when he wanted to describe an ionized gas that contained ions and electrons in about equal numbers so that the resultant space charge was very small [72]. However, already 1879, William Crookes observed a plasma in an experimental electrical discharge tube [26], but used the term *radiant matter* that dates back to Faraday's days in 1816 when he in a lecture hypothesized what lay beyond the conventional gas [65]. Phenomena related to plasma, however, have been known since the dawn of mankind [96, 9]. The most striking example visible to the human eye, often recurring in folklore, are probably the aurorae – the polar lights. In the 16th century, William Gilbert described the Earth as a giant magnet [44], and Gauss and Weber made detailed measurements of magnetic fluctuations, drawing the conclusion that the magnetic field around Earth was under influence from outside. A relationship between individual aurora and accompanying geomagnetic disturbances was noticed by Anders Celsius and Olof Peter Hiorter in 1747 [70]. In 1908, after a norwegian polar expedition, Kristian Kirkeland proposed the existence of electric currents going in and out of the polar regions along magnetic field lines [69]. The aurorae is the result of neutral molecules in the upper atmosphere being excited by the precipitating plasma particles, and subsequently emitting photons.

Another direct observation of a distant plasma phenomena was made in 1859, as Richard Carrington [15] and Richard Hodgson [57] independently witnessed an intense brightening of the Sun's surface which was accompanied by a disturbance in the geomagnetic field. This was the first recorded observation of a solar flare [3]. The Sun is in fact a brilliant example of how a plasma can be observed and studied remotely by the electromagnetic radiation that is emitted as a result of different plasma processes. Figure 1.1 shows a coronal mass ejection observed by NASA's Solar Dynamics Observatory. The light is emitted by charged particles that are accelerated and subsequently decelerated. As the charged particles will follow the magnetic field lines we are also able to observe the structure and topology of the magnetic field.

With the beginning of *in situ* measurements with the launch of a scientific instrument onboard a rocket reaching 117 km altitude by Van Allen in 1947, the area of space science started to make great progress [45]. Since then, numerous missions have been undertaken to further our understanding of our

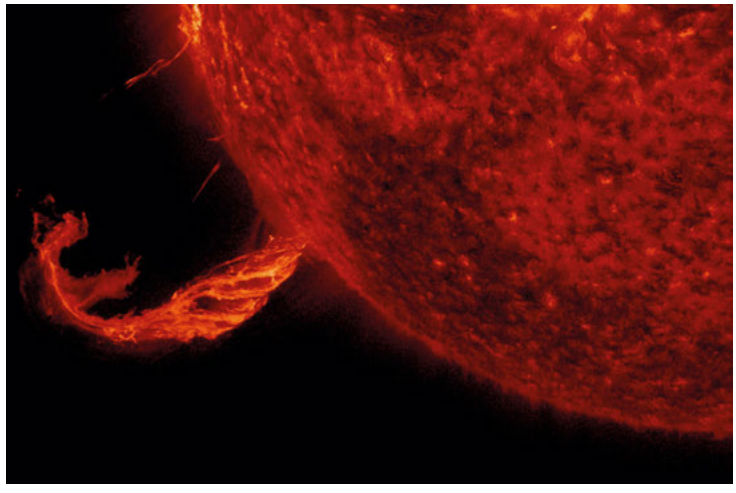

Figure 1.1. Coronal mass ejection seen in extreme ultraviolet light by the Solar Dynamics Observatory on February 24, 2015. Image Credit: NASA/Solar Dynamics Observatory[2].

near-Earth space environment. Today, plasma physics and space physics is a joint effort by theoreticians, space physicists, laboratory physicists, and simulation experts.

In this thesis, we study plasma phenomena that occur on scales where the details of electron dynamics become important, but may have large scale implications. The thesis is divided into two parts; the first part will give a basic introduction to the field while the second part consists of four peer-reviewed papers and one paper that is to be submitted

[2]https://www.nasa.gov/content/goddard/sdo/potw603-brief-outburst/index.html

2. Plasma environments

As most of the visible Universe consists of plasma, we are prone to encounter many different plasma environments. Quantities such as the density of the plasma (and any neutrals that are present), the temperature of the plasma, and the ambient magnetic field strength can vary with several orders of magnitude (Figure 2.1). The values of these quantities determine the spatial and temporal scales on which processes evolve. What mechanisms and processes that are important and dominates in a plasma, however, often does not depend on the absolute value of these quantities, but on their relative values (Figure 2.2). The parameter β describes the relative effect a plasma can have on the magnetic field, it is the ratio between the thermal and magnetic field pressures. The ratio between the plasma frequency $f_{p(e)} = \left(ne^2/m_e\varepsilon_0\right)^{1/2}$ and the cyclotron frequency $f_{ce} = eB/m_e$ describes the relative importance of plasma inertial effects and gyromotion in the magnetic field. This is why complementary studies of a plasma phenomenon can be conducted both in space and laboratory, even though the densities and temperatures can differ by several orders of magnitude. As the range of plasma parameters in our near space environment is large, the Earth's immediate space surroundings makes up an excellent laboratory, both to be studied in its own right, and to provide deeper understanding of plasma in general.

In this chapter we give a brief introduction to our near space environment and some laboratory environments.

2.1 The near-Earth space environment

The overall structure of our near-Earth space environment has been studied for several years using many spacecraft and ground based instruments, see e.g. Kivelson and Russel (1995) [70] and references therein. The space environment close to Earth consists of large regions of plasma that are rather uniform while remarkably different and distinct from each other (Table 2.1). This is noteworthy considering that the only sources of plasma to the magnetosphere is the solar wind and the ionosphere. The transfer of mass and energy between these different regions occur at thin extended boundaries that separate them. Also many processes related to plasma energization take place at these boundaries. Understanding the processes responsible for these processes is thus important in understanding for example the Sun-Earth interaction. Figure 2.3 shows the basic structures of the Earth's magnetosphere, including the

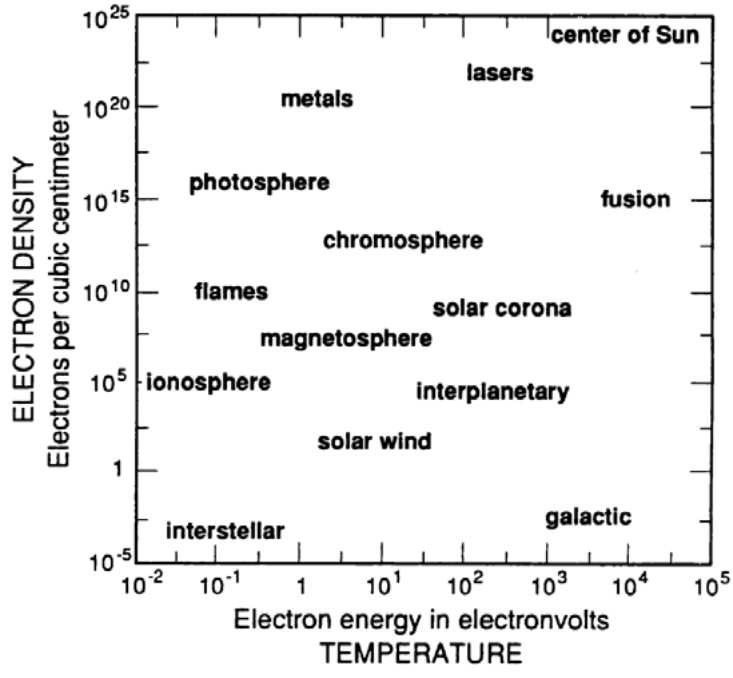

Figure 2.1. Electron density and temperature for different plasmas. Diagram adapted from Peratt (1996) [87].

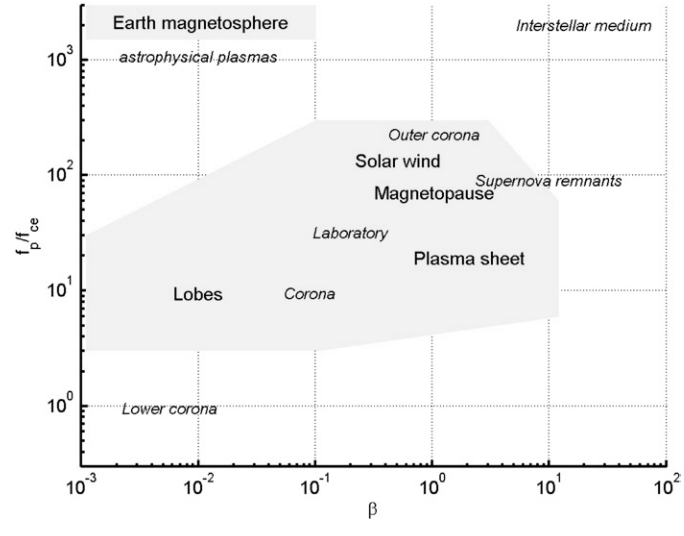

Figure 2.2. Dimensionless parameter space for a few environments in the Earth's magnetosphere and other plasmas. Diagram adapted from Vaivads et al. (2009) [110].

bowshock, magnetosheath, magnetopause, magnetosheath, tail current sheet, lobes, plasma sheet, which we will refer to below.

The plasma in the solar wind drift with a typical speed between 400 km/s and 800 km/s radially outward from the Sun [70]. It thus takes a typical solar wind particle $\tau_{SW} \approx 3.5$ days to reach Earth. During this transit time, the magnetic field is convected with the plasma flow. As the magnetic field is mapped to the rotating Sun, but is also tied to the plasma expanding radially, the magnetic field forms the so-called Parker spiral, which at the location of Earth has an angle of 45° with respect to the radial direction from the Sun. When the solar wind encounters the Earth's magnetosphere – the region around Earth that is dominated by the Earth's internal magnetic field – it is deflected. However, as the solar wind speed exceeds both the ion acoustic speed and the fast Alfvén speed, a quasi-stationary bowshock is first formed about two Earth radii (R_E) upstream of the Earth's magnetosphere. At the bowshock, the plasma is decelerated and heated and the density is increased [70]. The boundary between the magnetosphere and the plasma of solar wind origin is called the magnetopause while the region of shocked solar wind plasma between the bowshock and the magnetopause is called the magnetosheath. The structure of the bowshock and the magnetosheath behind it differs depending on the direction of the interplanetary magnetic field (solar wind magnetic field). If the magnetic field is approximately tangent to the shock surface, the shock is termed quasi-perpendicular, while if the magnetic field is more normal to the shock surface, the shock is termed quasi-parallel. The quasi-parallel bowshock, as well as the magnetosheath behind it is highly structured and dynamic [66], and reflected solar wind form a foreshock region extending out into the solar wind. In contrast, the quasi-perpendicular bowshock has less substructure, and the magnetosheath behind it is more quiet. The location of the magnetopause is decided by the balance of the dynamic pressure of the solar wind and the magnetic pressure of the magnetosphere. As the solar wind is highly variable the magnetopause – and in extension the bowshock – is not stationary, but tends to move back and forth. Somewhere close to the center of the dayside magnetopause – the subsolar point – the magnetosheath flow is stagnant. Further toward the flanks of the magnetopause where the plasma flow attains higher tangential velocities, shear driven instabilities such as the Kelvin-Helmholtz instability develop, leading to the formation of large scale vortices.

On the night side of Earth the magnetosphere is elongated, forming the magnetotail. The central region around the equatorial plane containing closed fields lines – the term closed field lines refers to field lines that are not connected to the solar wind, i.e. it has two footpoints in Earth, while open field lines refers to field lines that has one footpoint in Earth and one in the solar wind – is called the plasma sheet. To the south and north of the plasma sheet are the lobes, containing magnetic field lines with one footpoint in Earth, and the other in the solar wind, tailward of Earth. The plasma here can escape tailward and eventually join the solar wind. Since there is nothing that confines

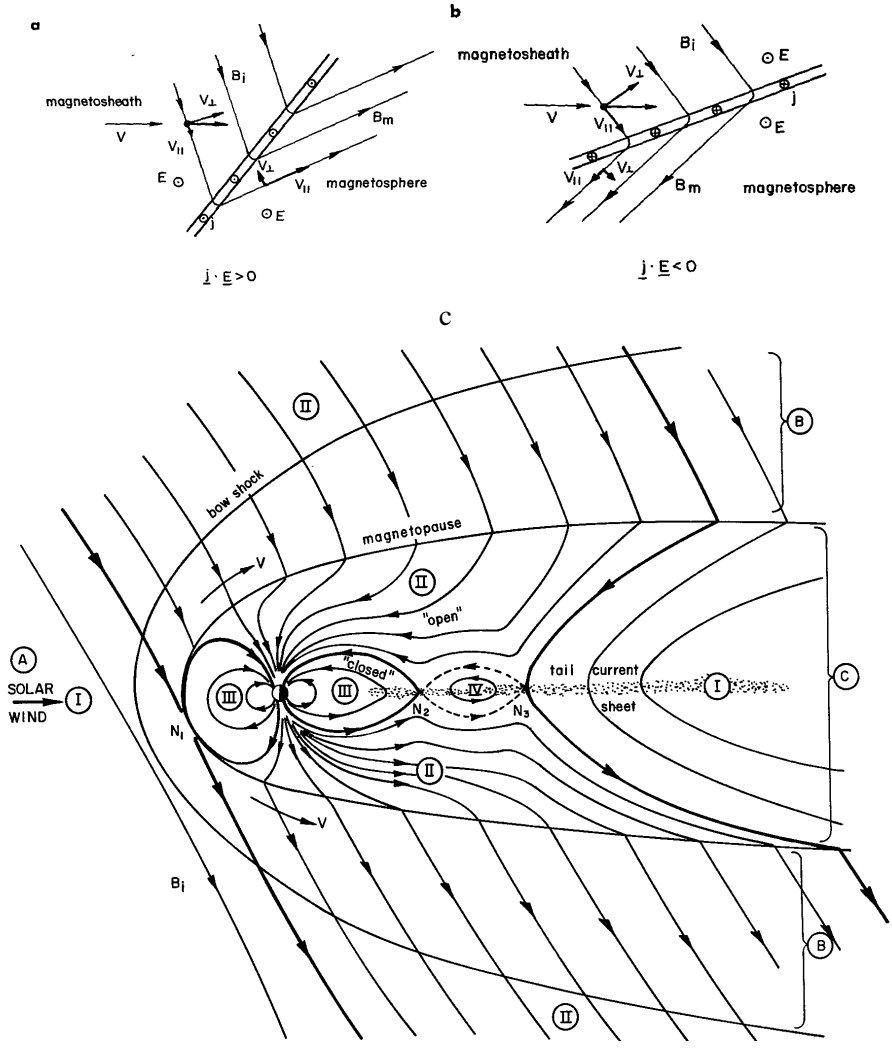

Figure 2.3. The solar wind magnetic field may connect to the magnetospheric magnetic field at the dayside magnetopause. The "open" magnetic field is convected with the plasma tailward, first releasing tension (see a) and then building it up (see b)[a]. In the magnetotail, the magnetic field can eventually reconnect again to form "closed" field lines. Adapted from Roederer (1979) [95]. The letters in (c) refer to (A) unperturbed solar wind, (B) shocked solar wind, or magnetosheath, and (C) magnetosphere. The roman numerals refer to regions with different magnetic connectivity. (I) The magnetic field connect directly to two footpoints on the Sun. (II) Magnetic field lines have one footpoint on the Sun, and one on Earth. (III) The magnetic field has two footpoints on Earth, and no direct connectivity to the interplanetary magnetic field. (IV) The magnetic field is completely embedded in the plasma.

[a] Or in the words of Roederer: *Anyone fond of the "moving field line picture" would "see" the fields lines collapse from both sides into the boundary [. . .] or emerge...*

Table 2.1. *Typical density, magnetic field and temperature in different plasma environments. The values, unless otherwise indicated, are taken from Kivelson and Russel (1995) [70].*

	n [cm^{-3}]	B[nT]	T_i [eV]	T_e [eV]
Ionosphere	10^6	$4 \cdot 10^4$	10^{-1}	1
Solar wind at 1 AU	5	5	1.2	1.5
Tail lobes	0.01	20	300	50
Plasma sheet	0.1-1	10	4000	600
Magnetosheath	10	15	150	25
Plasma sphere [27]	10^3	200	-	0.1
Radiation belts	1	$100-400$	10^4	10^4
ITER [62]	10^{14}	$4 \cdot 10^9$	-	-
MRX [113]	10^{14}	10^7	-	10

the plasma, the density in the lobes is typically much lower than in the rest of the magnetosphere (Table 2.1). The border between the plasma sheet and the lobes is called the plasma sheet boundary layer.

In the inner magnetosphere is a torus-shaped region of roughly co-rotating plasma originating from the ionosphere. The region is called the plasma sphere, and has an outer boundary varying between 4.5 R_E to 8 R_E [70]. Partly overlapping with this region [28] are the two radiation belts containing particles trapped in Earth's magnetic field, with energies much higher energy than in the rest of the magnetosphere trapped in Earth's magnetic field [111, 70].

The structure and dynamics of the boundaries between the various regions is highly variable and critical to the transport of mass and energy across them. The first model of the magnetopause current layer considered ions and electrons reflected as they encountered the magnetic field of Earth, resulting in a magnetopause thickness of one ion gyroradius. For a plasma with two dominant species of equal temperature, the current is divided into two layers, where the major part of the current is carried by the ions due to their larger gyroradius. Later studies found that the thickness was several ion gyroradii [6], and it was instead suggested that the balance of dynamic and magnetic pressure decided the thickness. Often, the magnetopause is not a smooth transition from the magnetosphere to the magnetosheath but contains substructures including small scale current sheets and magnetic flux ropes. Figure 2.4 shows an example of a magnetopause crossing observed by NASA's Magnetospheric Multiscale mission close to the subsolar point. The change in magnetic field occurs in several steps, associated with localized current sheets. Many of the current sheets are in addition associated with transitions between regions of different plasma. In Paper V, we study the thin current sheet observed between 07:19:20 and 07:19:22.

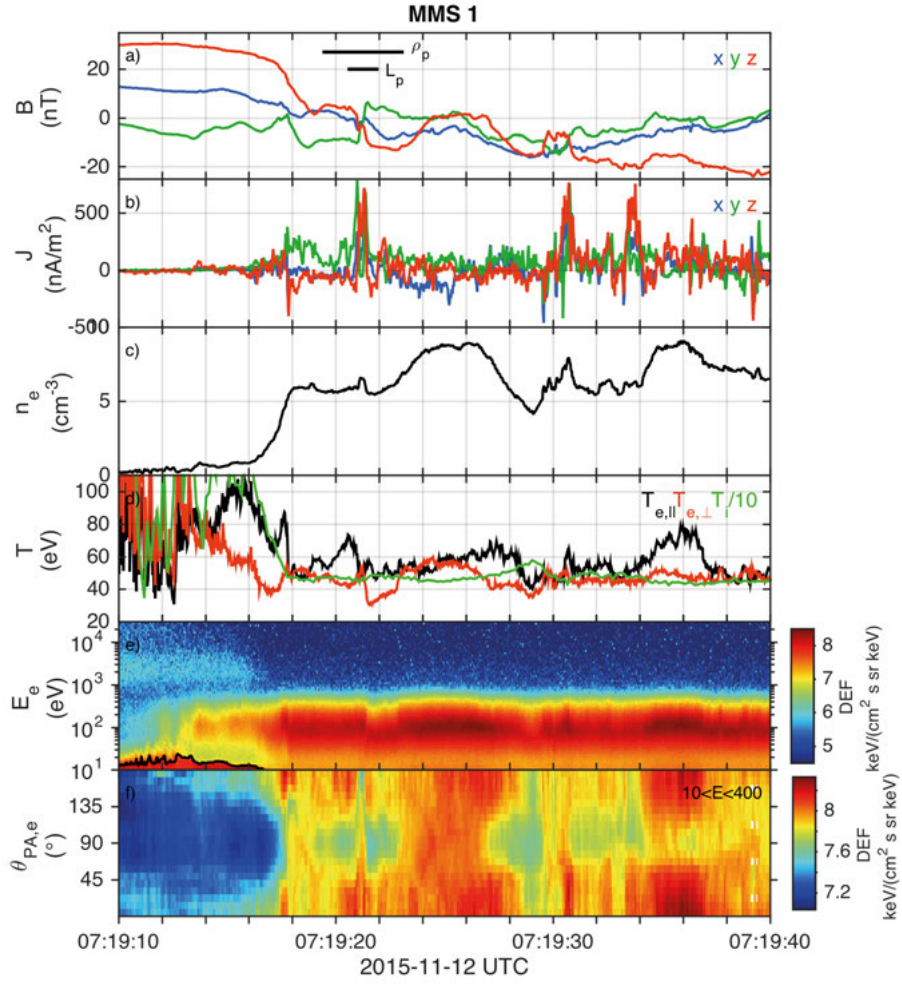

Figure 2.4. Magnetopause crossing close to the subsolar as seen by a spacecraft of the Magnetospheric Multiscale (MMS) mission. (a) Magnetic field. The ion gyroradius and inertial length are marked by black lines. (b) Current density. (c) Electron density. (g) Parallel and perpendicular electron temperatures, and ion temperature divided by 10. (g) Electron omni-directional differential energy flux. (f) Electron pitch-angle differential energy flux of energies between 10 eV and 400 eV. Figure partly adapted from Paper V.

Early it became clear that plasma from the shocked solar wind could penetrate the magnetic barrier set up by the Earth's magnetic field at the magnetopause. One process that enables plasma to pass between two magnetically separated regions is magnetic reconnection [90]. In this process, the magnetic field change connectivity, allowing stretched field lines to relax to a lower energy state. The energy is transferred from the magnetic field to particles. At the dayside magnetopause, this happens more efficiently during times when the solar wind magnetic field is directed southward, so that the magnetic fields on either side of the magnetopause are highly sheared (Figure 2.3). The reconnected magnetic field lines, convect with the plasma toward the nightside, adding magnetic flux to the magnetotail, making the cross tail current sheet thinner. The same process is also active in the magnetotail, where the sunward directed magnetic field north of the plasma sheet can reconnect with the tailward directed magnetic field to the south. Plasma from both the northern and the southern lobe is transported across the plasma sheet boundary layer, either being ejected Earthward joining the plasma sheet, or tailwards where it eventually mixes with the solar wind. In addition to this large scale scenario, reconnection can also occur in smaller regions along the magnetopause. For example, Kelvin-Helmholtz instabilities can generate vortices along the flanks of the magnetosphere, creating conditions favourable for reconnection to occur.

2.2 Laboratory environments

There are many laboratories dedicated to the study of fundamental plasma processes, but also to energy extraction through nuclear fusion. Laboratories present unrivaled opportunities to perform controlled, repeated experiments. The drawbacks include perturbative diagnostic devices – the probes used to measure the plasma is large with respect to the physical scales, and can give unnatural feedback–, boundary effects, and unwanted collisions. Generally, it is also hard to study the full course of natural events, as the experiments are often driven.

There are different kind of laboratories dedicated to investigating plasma processes. One is the Magnetic Reconnection Experiment (MRX)[113, 64] that uses merging or separation of toroidal magnetic fields to study magnetic reconnection [16]. Another is the LArge Plasma research Device (LAPD) [43], which produces a 10 m long plasma column well suited to study space related phenomena. It is especially compatible with ionospheric conditions, but also fit to study general phenomena that are ubiquitous in plasma, such as electron phase space holes [76]. The biggest, and most expensive plasma laboratory to date is under construction and is the International Thermonuclear Experimental Reactor (ITER) [62], dedicated to advancing the knowledge in

thermonuclear fusion [56] towards the goal of making it commercially feasible. It is a tokamak reactor [39] with a plasma volume of 840 m^3.

3. Observation of space plasmas

The study of space physics began with eyewitness accounts of aurora, and measurements of variations in the magnetic field with the compass needle. Diurnal variations in the magnetic field could eventually be attributed to currents flowing in a conducting upper atmosphere, in the region we now know as the ionosphere. In the beginning of the 20th century, the radio transmitter and receiver further allowed to probe the ionosphere by studying the reflection of radio waves in the different conducting layers. In the 1950's, in situ measurements commenced with the launch of rockets and satellites and many discoveries succeeded each other. [70] Today, the most advanced undertakings are often collaborations between both international and national space agencies, and involves hundreds of people, both experimentalists, theoreticians and numerical experts.

Although space missions become increasingly more sophisticated [45], interpreting in situ measurement can be a challenge. In addition, physical processes generally evolve both in space and time and can occur simultaneously on both global and local scales. The local scales can in turn be divided into multiple levels both in space and time as it often involves both electrons that are fast and light, and ions that in comparison are slow and heavy. For a solitary spacecraft there is one measurement point, which makes differentiation between spatial and temporal changes ambiguous. The need to distinguish between the temporal and spatial changes led to the launch of missions such as Cluster [38], and the Magnetospheric Multiscale (MMS) mission [11], which each consists of four spacecraft flying in formation. These are the satellites we have used in this thesis, and a brief introduction to them is given below.

3.1 The Cluster mission

The Cluster mission was launched by the European Space Agency in 2000[1] and is still operational (Figure 3.1). It was the first space mission consisting of four satellites flying in a tetrahedron formation. The satellites were launched into a polar orbit with perigee and apogee at ~ 4 and ~ 19 Earth radii, R_E, but has both actively, and due to the influence of the moon and the non-spherical Earth changed orbit many times. The orbital plane is fixed with respect to

[1] This was actually the second set of satellites built – Cluster II. Cluster I was launched in 1996 but was lost in the failed Ariane 5 maiden flight.

Figure 3.1. Two of the four Cluster satellites being prepared for launch. Image credit: ESA[3]

inertial space, allowing coverage of key plasma regions, such as the solar wind, bow shock, magnetopause, polar cusps, magnetotail and the auroral zones, during the course of one year. The main goal of the Cluster mission is to study plasma structures in three dimensions, and distinguishing between spatial and temporal variations in space. From an initial focus on a tetrahedron formation in parts of the orbit, the formation has changed during the years, in order to allow to focus on different phenomena.

The four Cluster satellites carry an identical set of 11 instruments (listed in Table 3.1), including particle detectors, magnetic and electric field instruments and spacecraft potential control devices.

Depending on the phenomena of interest, the satellites can operate in different sampling modes, sometimes dedicating more telemetry to special shorter periods, often called burst modes. Burst mode periods can either be scheduled to periods/regions where something in particular is expected to occur, such as a magnetotail or magnetopause crossing, or can be triggered by some special signal, such as a high amplitude electric field. During spacecraft burst mode (during $\sim$ 1 h), the electric and magnetic field is sampled at 450 Hz, instead of 25 Hz. As an example, a structure traveling with 1000 km/s, and that is 100 km long will be seen during 0.1 s. During the normal mode sampling rate, this would mean 2.5 samples for the whole structure, which might be enough to identify it, but not to study it in detail. Hence, in order to study certain small scale structures, which are traveling through space, it is necessary to utilize a higher sampling rate.

[3]http://sci.esa.int/cluster/22845-hoisting-of-rumba-above-tango/

Table 3.1. *Instrument suites of Cluster. For instrument details see Escoubet et al. (1997) and references therein.*

Instrument	Instrument range	Sampling rate
Cluster Ion Spectrometry (CIS) instrument	CODIF: H^+, He^+, He^{++}, O^+: ∼0-40 keV/e, HIA: 5 eV/e- 32 keV/e	full 3D: 4 s
Plasma Electron And Current Experiment (PEACE)	0.59 eV - 26.4 keV	one energy sweep 125 ms, full 3D 4 s
Research with Adaptive Particle Imaging Detectors (RAPID)	i^+: 40-4000 keV, e^-: 20-400 keV	full 3D: 2-4 s
Electric Field and Wave experiment (EFW)		25 Hz / 450 Hz / 9 kHz
Electric Drift Instrument (EDI)		observations every 120 ms / 16 ms
FluxGate Magnetometer (FGM)	DC - 10 Hz	15 Hz / 64 Hz
Spatio Temporal Analysis of Field Fluctuations (STAFF) experiment	>10 Hz	waveform 450 Hz/9 kHz, spectra 8 Hz - 4kHz at 0.125s-4s
Waves of HIgh frequency and Sounder for Probing of Electron density by Relaxation (WHISPER)	450 Hz	2/8 kHz)
Wide Band Data (WBD)	B: 0.1-9.5 kHz, E: 0.1-77 kHz	

Figure 3.2. The Magnetospheric Multiscale satellites being processed for launch. Image Credit: NASA/Ben Smegelsky[5].

3.2 The Magnetospheric Multiscale (MMS) mission

The Magnetospheric Multiscale (MMS) mission [11] was launched in 2015 and targets the electron diffusion region of magnetic reconnection (Figure 3.2). Magnetic reconnection predominantly occurs where the magnetic shear is the largest [104]. Therefore, as MMS needs to spend as much time as possible close to the EDR, it has an equatorial orbit, with apogee located close to the expected magnetic reconnection location [42]. At the dayside this is at the magnetopause, which is the target for the first phase of the mission (Figure 3.3). The second phase will target the magnetotail.

The mission consists of four identical satellites with a formidable suite of instruments making in situ measurements of electromagnetic fields and thermal as well as energetic particles. The set of instruments is listed in Table 3.2. The physical length scale of the electron diffusion region is on the order of the electron inertial length, which at the magnetopause can be a few km. At the same time, the electron diffusion region is typically not stationary, but can both oscillate and convect. At the magnetopause, the normal velocity of the electron diffusion region is associated with the magnetopause motion, which can be tens of km/s. For an electron diffusion region of width 5 km and velocity of 50 km/s, the dwell time of MMS within the electron diffusion region is only 0.1 s (neglecting motion tangential to the magnetopause as the electron diffusion region is typically more extended in this direction), which constraints the measurement requirements. For MMS to sample at least three full 3D electron distributions within a EDR as described above, the sampling rate has to be 0.03 s^{-1} [11].

[5]https://www.nasa.gov/content/magnetospheric-multiscale-observatories-processed-for-launch

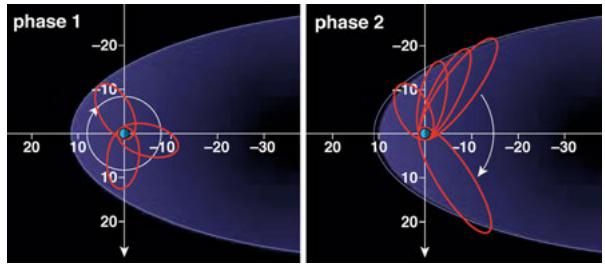

Figure 3.3. The first and second phase of the MMS mission, covering the dayside magnetopause and the magnetotail respectively. The dayside magnetopause reconnection region is studied for two consecutive years, 2015 and 2016, whereafter the apogee is increased to study magnetotail reconnection. Image adapted from Burch et al. (2015) [11].

The highest data rates of MMS results in about 1 Gbit every 5 minutes, allowing for only 20 minutes of data with this quality to be downlinked every orbit. Therefore MMS employs a system where a so-called Scientist In The Loop (SITL) daily monitors survey data of lower sampling rates and assigns figures of merits (FOM) to different time intervals depending on their presumed scientific interest. High sampling rate data with high FOM's are thereafter downlinked during the subsequent orbits. These data intervals are typically a few minutes long.

Table 3.2. *Instrument suites of MMS (we list the most common data products). For instrument details see Burch et al. (2015) and references therein.*

Instrument	Instrument range	Sampling rate
Fast Plasma Investigation (FPI)	10 eV-30 keV	electrons: 30 ms, ions: 150 ms
Hot Plasma Composition Analyzer (HPCA)	H^+, He^{++}, He^+ 1 eV - 40 keV	full 3D
Energetic Ion Spectrometer (EIS)	H^+: 20keV to >0.5MeV	full 3D: 20 s
Fly's Eye Energetic Particle Spectrometer (FEEPS)	ions: 45 keV - 650 keV, electrons: 25 keV - 650 keV	64 samples per spacecraft rotation ($\sim$ 20 s)
Electric field Double Probes (EDP) and Axial Double Probes (ADP)		8 kHz
Electric Drift Instrument (EDI)		16 Hz / 125 Hz
FluxGate Magnetometer (FGM)		128 Hz
Search Coil Magnetometer (SCM)		1 Hz - 6 kHz

4. Motion of charged particles in electromagnetic fields

The force on an electrically charged particle due to an electric field **E** and a magnetic field **B** is given by

$$\mathbf{F} = q\left(\mathbf{E} + \mathbf{v} \times \mathbf{B}\right), \tag{4.1}$$

often called the Lorentz force where q is the electric charge, and **v** is the velocity of the particle. The resulting acceleration [22] of a particle with mass m is given by

$$m\frac{d\mathbf{v}}{dt} = q\left(\mathbf{E} + \mathbf{v} \times \mathbf{B}\right). \tag{4.2}$$

In the following we ignore interactions that in other environments are important, or even dominate. For example, collisions and gravity can be neglected since plasma in near-Earth space above the ionosphere is essentially collisionless and the particles we discuss have energies well above the escape velocity of Earth.

Since both **E** and **B** can be both space and time dependent, the trajectories can become complicated and may depend strongly upon initial conditions. This may cause closely located particles of similar velocities to follow strongly divergent paths. For certain situations the particle trajectories can be described and predicted in more convenient ways, without having to follow the particle path and acceleration history. These descriptions are an important aid in understanding particle kinetics where individual particle trajectories are impossible to follow. In the following sections, we describe a few selected types of models.

4.1 Guiding center drift

In a uniform magnetic field, charged particles will trace circular orbits at an angular frequency often referred to as the gyrofrequency $\omega_c = qB/m$ at the radius $\rho = v_\perp/\omega_c$. If the magnetic field is inhomogeneous, or if there are electric fields present, the trajectories will become distorted and may result in a net drift. If the drift can be well approximated by the translatory motion of the guiding center – the point to which the instantaneous curvature radius points – this is called a guiding center drift.

The simplest example is when a uniform electric field that has a component perpendicular to the ambient magnetic field **B** is present. During the part of the orbit where the electric field acts to accelerate the particle, the instantaneous gyroradius is increased, whereas it is decreased during the part of the orbit where the electric field acts to decelerate the particle. The resulting guiding center velocity is given by

$$\mathbf{v}_{\mathbf{E}\times\mathbf{B}} = \frac{\mathbf{E}\times\mathbf{B}}{B^2}. \tag{4.3}$$

and is illustrated in Figure 4.1 for electrons. As $\mathbf{v}_{\mathbf{E}\times\mathbf{B}}$ does not depend on the particle mass nor the charge, it is equal for ions and electrons. There is thus no current associated with this kind of drift motion. Similar distortions of the trajectory can also arise due to perpendicular gradients in the magnetic field, where the orbit will be tighter in the region of larger magnetic field. In this case, the guiding center drift of electrons and ions deviate, resulting in a net current.

The guiding center description becomes less effective and eventually breaks down when either the rate of temporal changes or the gradient length scales of **E** and/or **B** approach the gyroradius of the particle. This typically occurs first for the ions due to their larger mass. There are thus situations when the electrons $\mathbf{v}_{\mathbf{E}\times\mathbf{B}}$ drift and the ions do not. This behaviour was observed in Paper I for the case of lower hybrid waves in the plasma sheet boundary layer (Figure 4.1). Lower hybrid waves have perpendicularly polarized electric field and wavelengths typically larger than ρ_e but well below ρ_i. The $\mathbf{v}_{\mathbf{E}\times\mathbf{B}}$ drift of electrons thus gave rise to a net current associated with observable parallel magnetic field fluctuations.

In large volumes of space, the guiding center theory provides a good estimate of the particle motion. However, as we are especially interested in processes occurring at boundaries between different plasmas where the magnetic field often changes in amplitude and direction on short spatial scales, we need additional descriptions of the particle motion than the guiding center theory. In the following section we will consider the periodic motion of charged particles in a non-uniform one-dimensional magnetic field.

4.2 Periodic motion in non-uniform magnetic

The motion of a charged particle in a prescribed electromagnetic field can be described using the constants of motion [51], which are the total energy of the particle

$$H_s = \varepsilon + q\phi = \frac{m_s}{2}\left(v_x^2 + v_y^2 + v_z^2\right) + q\phi \tag{4.4}$$

and the different components of the canonical momenta

$$p_x = mv_x + qA_x, \tag{4.5}$$

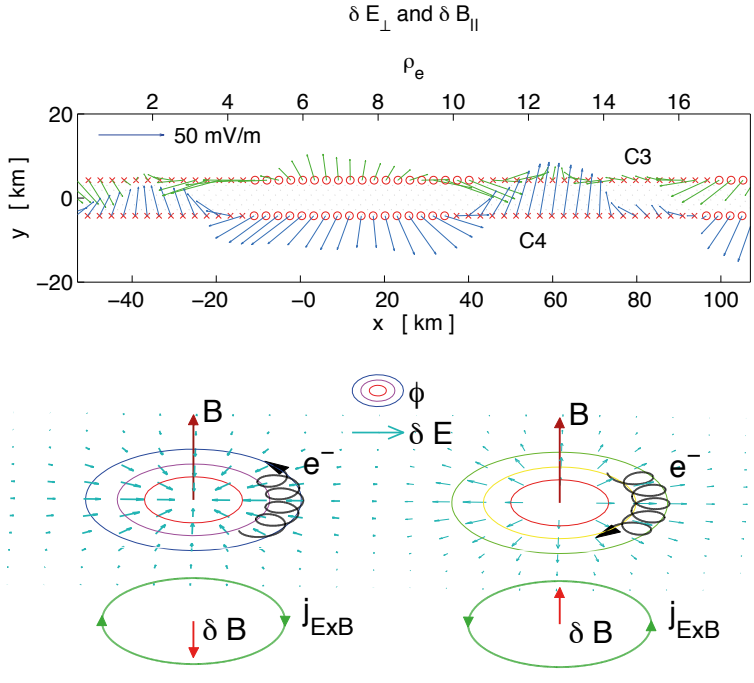

Figure 4.1. Electron $\mathbf{v_{E\times B}}$ drift in lower hybrid wave field electric field. (top) Perpendicular wave electric field and (anti)parallel ($\times/\circ$) wave magnetic field observed by the two satellites Cluster 3 (green) and Cluster 4 (blue). The ambient magnetic field is directed out of the plane. (bottom) Illustration of electron motion and resultant current and wave magnetic field due to the wave electric field and ambient magnetic field. Figure adapted from Paper I.

$$p_y = mv_y + qA_y, \tag{4.6}$$
$$p_z = mv_z + qA_z, \tag{4.7}$$

where $A_{x,y,z}$ are the different components of the vector potential and ϕ is the electrostatic potential. For a one-dimensional magnetic field configuration given by

$$\mathbf{B} = B_0 \frac{z}{L}\hat{\mathbf{x}} \quad \text{and} \quad \mathbf{B_g} = B_g\hat{\mathbf{y}}, \tag{4.8}$$

the components of the vector potential are given by

$$A_x = B_g z, \quad A_y = -\tfrac{B_0}{2L}z^2, \quad A_z = 0. \tag{4.9}$$

This is a simplified but general model of a current sheet, i.e. the transition between two regions with differently directed magnetic fields. Neglecting the displacement current in Ampère's law, the associated current is given by $\mathbf{J} = B_0/\mu_0 L\hat{\mathbf{y}}$. The angle between the asymptotic magnetic fields is often referred to as the magnetic shear angle. The magnetotail cross field current is typically characterized by roughly antiparallel magnetic fields (directed sunward to the north and anti sunward to the south of the magnetic equatorial plane) in which the guide field B_g is close to zero. In contrast, at the dayside magnetopause the magnetic shear angle strongly depends on the solar wind conditions and B_g is typically finite.

Based on the vector potentials given by (4.9), the equation of motion in the normal direction becomes

$$m\frac{dv_z}{dt} = -\frac{\partial \Lambda}{\partial z} \tag{4.10}$$

where the effective potential Λ is given by

$$\begin{aligned} \Lambda &= \frac{1}{2m}\left[(p_y - qA_y)^2 + (p_z - qA_z)^2\right] + q\phi(z) \\ &= \frac{1}{2m}\left[\left(p_y + q\frac{B_0}{2L}z^2\right)^2 + (p_z + qB_g z)^2\right] + q\phi(z). \end{aligned} \tag{4.11}$$

and describes the periodical motion in the normal direction. The character of the trajectory depends on the particle energy and can be divided into two general groups: crossing and non-crossing trajectories. For the present current sheet which has a local maximum at $z = 0$ (assuming the electrostatic potential is symmetric about $z = 0$), this becomes:

$$\varepsilon + q\phi > \Lambda_{z=0} = \frac{p_y^2}{2m} + \frac{p_z^2}{2m} + q\phi_{z=0} \quad \rightarrow \quad \text{crossing} \tag{4.12}$$
$$\varepsilon + q\phi < \Lambda_{z=0} = \frac{p_y^2}{2m} + \frac{p_z^2}{2m} + q\phi_{z=0} \quad \rightarrow \quad \text{non-crossing} \tag{4.13}$$

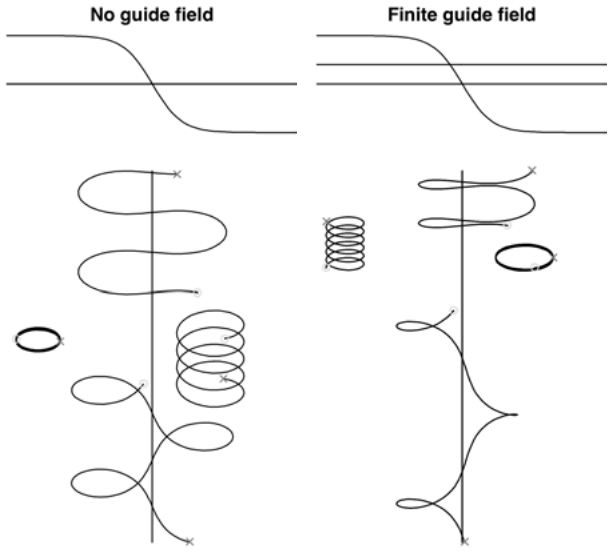

Figure 4.2. Particle orbits in current sheet with and without guide field. The guide field makes the orbit asymmetrical about the central plane.

If the energy is large enough to overcome the potential barrier, the particles will cross to the other side. Figure 4.2 illustrates trajectories for a few particles of varying energies in a current sheet with and without guide field, and vanishing electrostatic potential $\phi = 0$. The effect of a guide field is to more strongly confine particles to either side, as it will keep the particles more strongly magnetized. Electron motion of this type is discussed in Paper V when studying a current sheet of width comparable to the electron gyroradius. As a contrast to the periodic orbits that occur when the magnetic field is tangential, including a finite normal magnetic field component will make the orbits irregular. This is illustrated in Figure 4.3, where the magnetic field model is based on data observed by MMS1, and the sample electrons are chosen from the observed electron distribution.

4.3 Particle trapping in wave electric field

Electric and magnetic fields are in general both space and time dependent. This may cause particles that are initially free, to become trapped, if a field perturbation is growing. In this section we will consider the motion of a charged particle in a one-dimensional cosine electrostatic potential field, $\phi = \phi_0 \cos(kx - \omega t)$. The phase velocity of the wave is given by $v_{ph} = \omega/k$, and the corresponding electric field is $\mathbf{E} = -\phi_0 k \sin(kx - \omega t)\hat{\mathbf{x}}$. As the particle moves

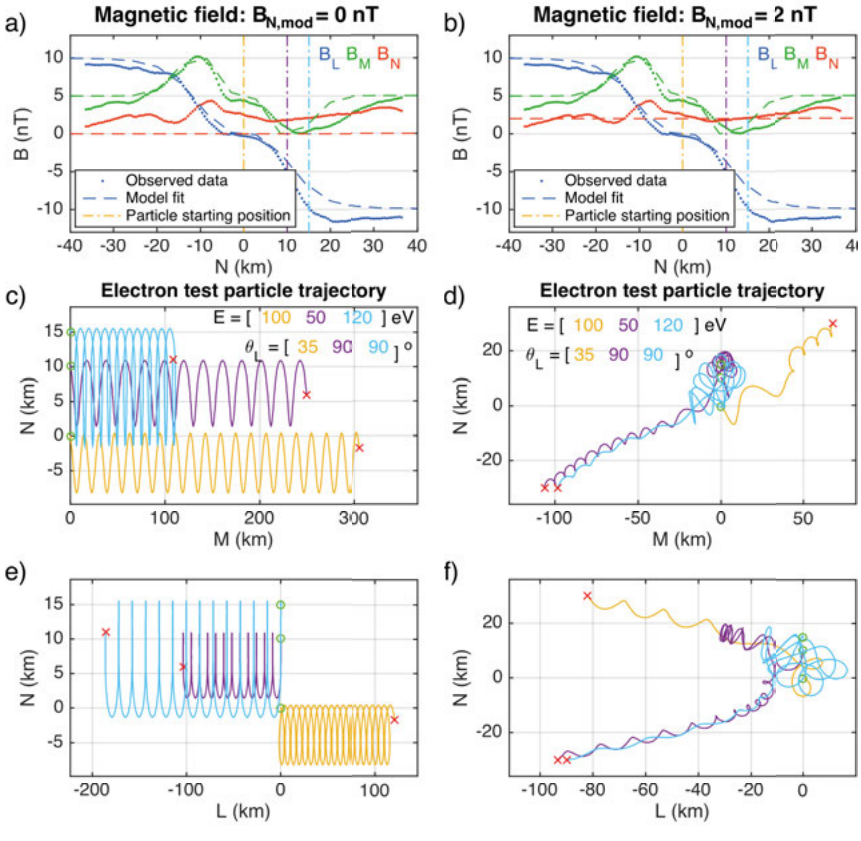

Figure 4.3. Electron test particle trajectories based on data from MMS1, for $B_{N,mod} = 0$ (left) and $B_{N,mod} = 2$ nT (right). (a)-(b) Observed (dotted) and model (dashed) magnetic field. The vertical dotted-dashed lines mark the starting points of the electrons. (c)-(d) Electron trajectories in the NM plane, and (e)-(f) NL plane. A finite normal magnetic field introduces chaotic trajectories and enables electrons to escape from the current sheet. Figure adapted from Paper V.

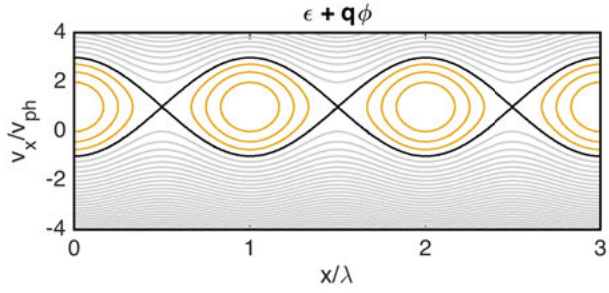

Figure 4.4. Illustration of trajectories in phase space of a negatively ($q < 0$) charged particle. The lines are contours of constant energy, which the particles follow, in the presence of a traveling sine electric field wave. Trajectories of free (gray), marginally trapped (black) and trapped (yellow) particles are seen. If the wave amplitude grows in time, particles traveling on trajectories just outside the line for marginally trapped particles will become trapped.

in the electrostatic potential field, the energy will be transferred back and forth between kinetic and potential energy, $\varepsilon \leftrightarrow q\phi$, modulating the particle speed. This is illustrated in Figure 4.4, which shows contours of constant energy in a one-dimensional phase space. There are two general types of trajectories, depending on whether or not the energy of the particle is large enough to overcome the potential barrier of the wave. It is convenient to move to the reference frame of the wave:

$$\frac{m}{2}(v_x - v_{ph})^2 + q\phi < (q\phi)_{max} \rightarrow \text{ trapped} \tag{4.14}$$

$$\frac{m}{2}(v_x - v_{ph})^2 + q\phi > (q\phi)_{max} \rightarrow \text{ passing} \tag{4.15}$$

Particles moving along closed contours are trapped and oscillates in the wave field around the phase velocity. If the wave field is growing, a particle that are on an initially open contour may end up on a closed contour, becoming trapped. If a considerable amount of particles are within a certain velocity range in phase space, many particles will be trapped approximately simultaneously, leading to many particles on a certain trajectory. This leads to holes in phase space, referred to as electron and/or ion phase space holes. The phase space holes are associated with propagating density depletions of the respective species, accompanied by divergent or convergent electric fields. As particle trapping may significantly alter the particle distributions, it is in some cases associated with irrevocable heating of the trapped population [20]. The trapping may also lead to a reduction in the current depending on which parts of the distributions becomes trapped, see Figure 4.5.

Electrostatic solitary waves, which may be associated with particle trapping and phase space holes, are ubiquitous in nature, and manifestations of strongly nonlinear processes. For a long time, before it came customary to sample waveforms in space, they were often interpreted as broadband turbu-

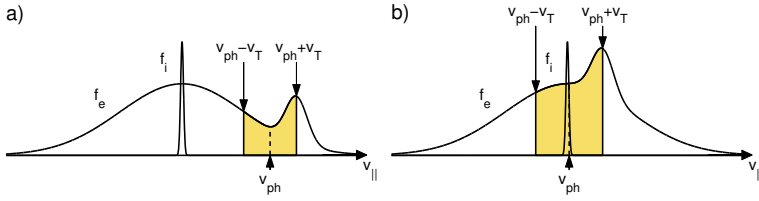

Figure 4.5. Illustration of trapping range at instability saturation (shaded area) for two different plasmas generating waves at different phase velocities. (a) The wave affects only the electrons, approximately the same amount which have $v > v_{ph}$ and $v < v_{ph}$, resulting in little change in the total current. (b) The wave trapping range may affect both the ions and electrons. In this case the trapping of electrons is highly asymmetrical, which may result in a significant reduction in the total current. Adapted from Paper III.

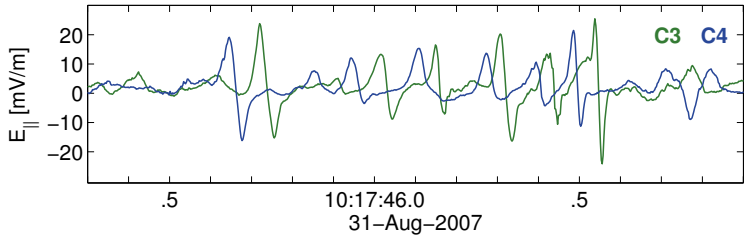

Figure 4.6. Observation of electrostatic solitary waves by two Cluster satellites in the plasma sheet boundary layer. The electric field is divergent, consistent with electron phase space holes.

lence, but were subsequently identified as sharp dipolar spikes in the electric field data [79]. Following this, observations have been made in many different plasma, including space [67, 19, 103, 78, 89] and laboratory [40, 77]. Electron holes are also widely studied using numerical simulations [74, 35, 21], and are often regarded as signs of strong instabilities and energetic processes. The electrostatic waves studied in Paper II were found to have divergent fields, consistent with electron phase space holes (Figure 4.6). Electrostatic solitary waves were also studied in Paper III.

4.4 Adiabatic particle motion

While charged particles are strongly confined in the direction perpendicular to the magnetic field due to the magnetic force, they are often left relatively free to drift in the direction parallel to the magnetic fields. However, if the magnetic field diverges or converges such that the magnetic force during one gyro orbit is not always in the same plane, the net force will have a component parallel to the direction of the average magnetic field. If the particle experiences a

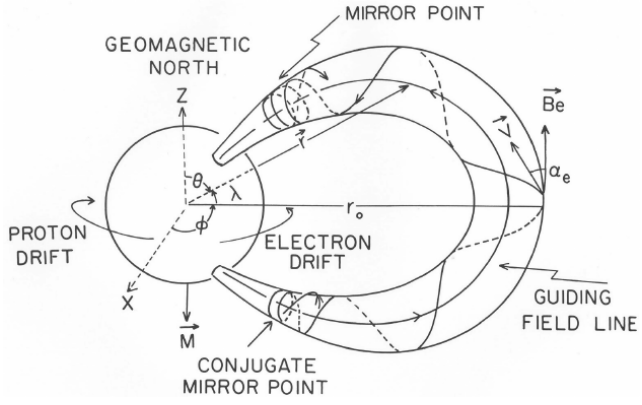

Figure 4.7. Motion of particles trapping the dipole field of Earth. Picture adapted from Adel (2008) [1].

convergent field, the force will be opposite to the particle motion while if the particle experiences a diverging magnetic field the force will be in the same direction as the particle motion. This is often referred to as the magnetic mirror force as particles are repelled if they move into a region of stronger magnetic field. By combining two mirrors, a particle can be trapped, bouncing back and forth between the mirror points. For example, this happens for particles in the dipole field of Earth, which is illustrated in Figure 4.7.

If the magnetic field as observed by the particle converges or diverges slowly enough, the first adiabatic invariant

$$\mu = \frac{mv_\perp^2}{2B}, \tag{4.16}$$

which is the magnetic moment of the particle, will be conserved. If μ is indeed conserved, a change in the magnetic field B has to be accompanied by a change in the perpendicular kinetic energy and velocity, while the total kinetic energy

$$W = \frac{mv_\perp^2}{2} + \frac{mv_\parallel^2}{2}, \tag{4.17}$$

is conserved. This implies that the pitch angle θ – the angle between the magnetic field and the particle velocity – has to change:

$$\frac{\sin^2\theta_1}{B_1} = \frac{\sin^2\theta_2}{B_2}. \tag{4.18}$$

The angle

$$\theta_2 = \sin^{-1}\left(\sqrt{\frac{B_2}{B_1}}\sin^2\theta_1\right) \tag{4.19}$$

thus describes the broadening or narrowing of the particle pitch angle distribution in a changing magnetic field. Reflection occurs at $\theta_2 = 90^\circ$, when

$$\sin^2 \theta_1 = \frac{B_1}{B_2}. \tag{4.20}$$

Therefore, for a given energy, particles with a larger initial pitch angle are reflected at weaker magnetic fields. If the maximum amplitude of the magnetic field along the path of the particle is weaker than the field required for reflection $B_{max} < B_2 = B_1 / \sin^2 \theta_1$, the particle will be able to pass this bottle neck. It is also possible that the pitch angle changes due to non-adiabatic processes, for example collisions or wave-particle interactions. This is common for particles trapped in the Earth's magnetic dipole field. When particles reach the upper atmosphere they may experience multiple collision and loose energy, and not be able to enter the magnetosphere again. Particles that move into a stronger magnetic field but are not trapped are said to belong to the loss cone.

As it is impossible to follow the exact trajectory of a particle in any experiment or natural setting, in practice the magnetic moment has to be calculated for an ensemble of particles. Thereafter, the observed temporal or spatial changes in the particle distribution can be compared to the adiabatic predictions, for example the variation in pitch angle described by Eq. 4.19. To investigate the adiabatic behaviour of different parts of the particle distribution, one can for example calculate the thermal speed for different energy ranges.

In Paper V we investigate the adiabatic versus non-adiabatic behaviour of electrons inside and in the vicinity of a reconnecting (see Section 7.2) current sheet at the dayside magnetopause (Figure 4.8). The magnetic moment calculated from the perpendicular thermal speed of the electrons was approximately constant both before and after the crossing of the current sheet. In the center of the current sheet, the magnetic moment was increased and not constant. The non-constancy of the magnetic moment at the center of the current sheet is consistent with the observed length scales: as the length scale of magnetic field gradient was comparable to the electron thermal gyroradius (Figure 4.8b), a substantial part of the electrons can not perform a well-defined gyromotion. However, by looking at the pitch-angle distribution in Figure 4.8g, we can see that in the center of the current sheet the electrons were partially trapped in the magnetic field depression: the broadening/narrowing of the pitch-angle distribution was partly[1] followed by the adiabatic prediction given by Eq. 4.19 (see the dashed line). Examples of particle trajectories based on observed data for this event are shown in Figure 4.3. We note that the maximum magnetic field amplitude is smaller on the left side of the current sheet that on the right side of the current sheet, which should allow electrons to more easily escape in

[1]For an example of when the broadening of the pitch angle distribution was very well described by the adiabatic approximation (Eq. 4.19), see [75], which investigates the same event as studied in Paper IV.

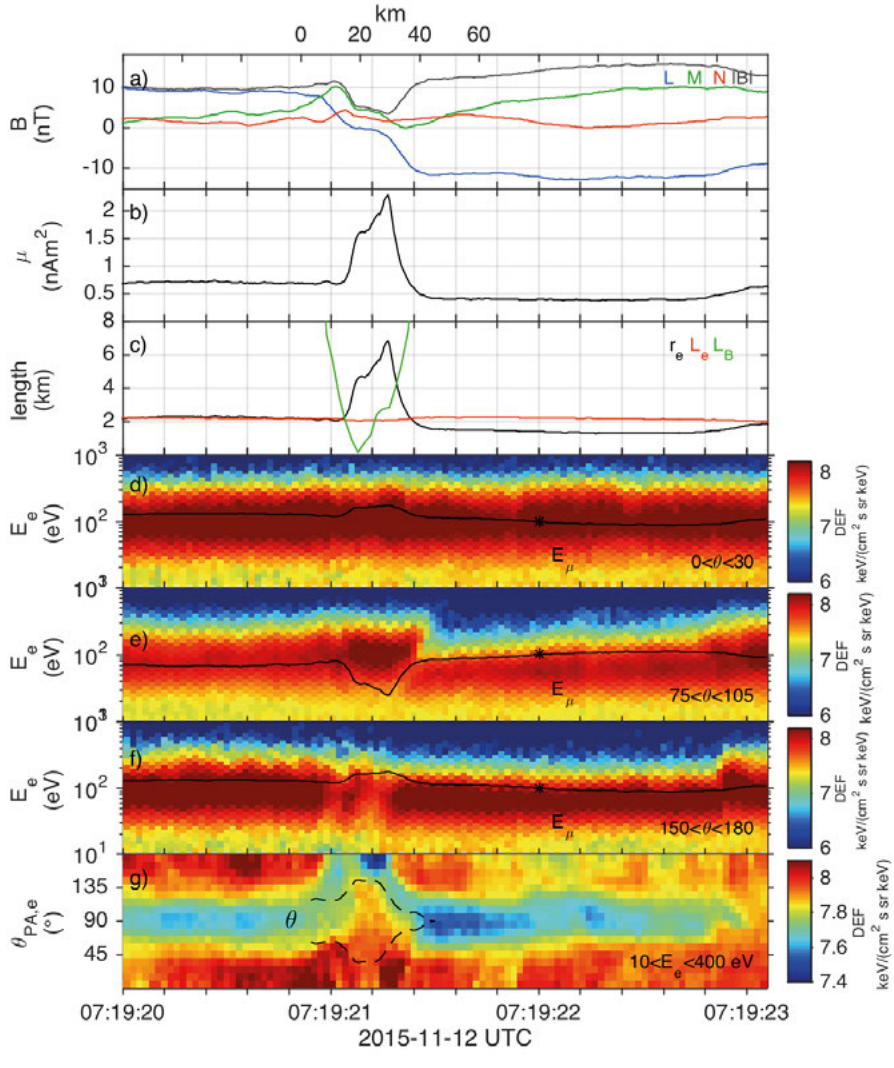

Figure 4.8. Current sheet crossing observed by a satellite of the Magnetospheric Multiscale mission at the dayside magnetopause. (a) Magnetic field, (b) Magnetic moment. (c) Electron gyroradius and magnetic length scale $L_B = \mu_0^{-1}|B_L|/|J_M|$. (d)-(f) Electron differential energy flux at three different pitch angle ranges θ; $[0°, 30°]$ (parallel), $[75°, 105°]$ (perpendicular), and $[150°, 180°]$ (antiparallel). The black lines mark the expected variation in (anti)parallel and perpendicular energy fluxes if the electrons behave adiabatically, see Eq. 4.22. (g) Pitch-angle distribution of electron differential energy flux in the energy range 10 to 400 eV. The dashed lines mark the expected variation in pitch angle for adiabatic electrons, see Eq. 4.19. Both before and after the current sheet crossing, the magnetic moment is approximately constant. Figure adapted from Paper V.

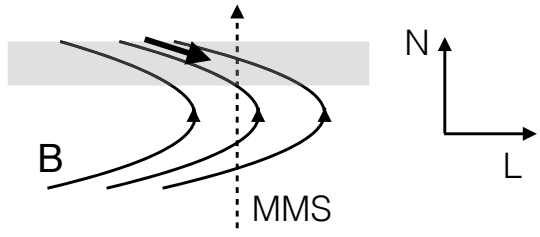

Figure 4.9. Sketch of the current sheet crossing shown in Figure 4.8. The dashed line shows the satellite trajectory as it crosses the current sheet (omitting any tangential motion). The gray shaded area indicates the region of constant magnetic moment observed between 07:19:21.4 and 07:19:22.8. The thick arrow shows the motion of the adiabatic electrons along the magnetic field.

this direction. This seems to be the case as the perpendicular distribution is somewhat depleted there (green/yellow area within the dashed line).

We now look at the region on the right side of the current sheet, where the magnetic moment was approximately constant for about 1.5 s. If the electrons behave adiabatically, the energy levels should depend on the magnetic field amplitude according to

$$E_\perp(t) = \frac{1}{2}mv_\perp(t)^2 = \frac{1}{2}\frac{mv_\perp^2}{B}B(t) = \frac{E_{\perp,\mathrm{ref}}}{B}B(t), \tag{4.21}$$

$$E_\parallel(t) = E_{\parallel,\mathrm{ref}} + E_{\perp,\mathrm{ref}} - \frac{E_{\perp,\mathrm{ref}}}{B}B(t). \tag{4.22}$$

Here, the perpendicular and antiparallel energy flux change in accordance to the adiabatic prediction, while the parallel energy flux remains approximately constant. In Paper V this was interpreted as electrons being cooled adiabatically in the perpendicular direction while approaching the current sheet, see Figure 4.9.

We end this section by trying to make a possibly complicated story simple, based on the observation related above. Let us consider an electron starting on the right hand side of the current sheet in Figure 4.8 (or top of the current sheet in Figure 4.9). This is what might happen to it. (1) The electrons move adiabatically in toward the current sheet and gradually shift pitch angle toward 180°. (2) At the center of the current sheet, the electrons bounce in the curved magnetic field in such a way that the pitch angle is not conserved. (3) As the magnetic field is lower on the opposite side from where they entered, they can more easily exit in this direction, and will gradually be shifted toward pitch angle 180° again. In this way the electrons are funneled from one side of the current sheet to the other. The story of the parallel (pitch angle 0°) electrons will have to wait for another day.

5. Plasma descriptions

The fundamental laws which govern electromagnetic interactions are Maxwell's equations that were established in their current collected form by James Clerk Maxwell in 1861-1862 [80]:

$$\nabla \cdot \mathbf{E} = \frac{\rho}{\varepsilon_0} \tag{5.1}$$

$$\nabla \cdot \mathbf{B} = 0 \tag{5.2}$$

$$\nabla \times \mathbf{E} = -\frac{\partial \mathbf{B}}{\partial t} \tag{5.3}$$

$$\nabla \times \mathbf{B} = \mu_0 \mathbf{J} + \mu_0 \varepsilon_0 \frac{\partial \mathbf{E}}{\partial t} \tag{5.4}$$

where ρ is the charge density, $\mathbf{J}$ is the current density and μ_0 and ε_0 are the permittivity and permeability of free space, respectively. The equations describe how electric and magnetic fields interact self-consistently with charges and currents, which are often referred to as sources. The current and charge densities are in the most general case given by

$$\mathbf{J} = \sum_s q_s n_s \mathbf{v_s}, \quad \text{and} \quad \rho = \sum_s q_s n_s \tag{5.5}$$

where the sum is over all plasma particles. To keep track of all the individual particles and the fields they produce is however a tedious task. It is more convenient to treat the particles in a statistical manner, using a particle distribution function $f = f(\mathbf{r}, \mathbf{v}, t)$, that describes the probability density of finding a particle at point $\mathbf{r}$ with velocity $\mathbf{v}$ at time t. The 6D space spanned by $\mathbf{r}$ and $\mathbf{v}$ is called phase space. The evolution of the plasma distribution function is governed by the Boltzmann equation,

$$\frac{df}{dt} = \frac{\partial f}{\partial t} + \mathbf{v} \cdot \nabla f + \frac{q}{m} (\mathbf{E} + \mathbf{v} \times \mathbf{B}) \cdot \frac{\partial f}{\partial \mathbf{v}} = \left(\frac{\partial f}{\partial t} \right)_c + \left(\frac{\partial f}{\partial t} \right)_{other}, \tag{5.6}$$

where $\left(\frac{\partial f}{\partial t} \right)_c$ describes the change in the distribution due to collisions, $\left(\frac{\partial f}{\partial t} \right)_{other}$ describes any other effects or sources, and

$$\frac{d\mathbf{v}}{dt} = \frac{q}{m} (\mathbf{E} + \mathbf{v} \times \mathbf{B}) \tag{5.7}$$

is the time rate of change of the velocity of a particle of the distribution due to the electromagnetic forces acting upon it. In the absence of collisions and

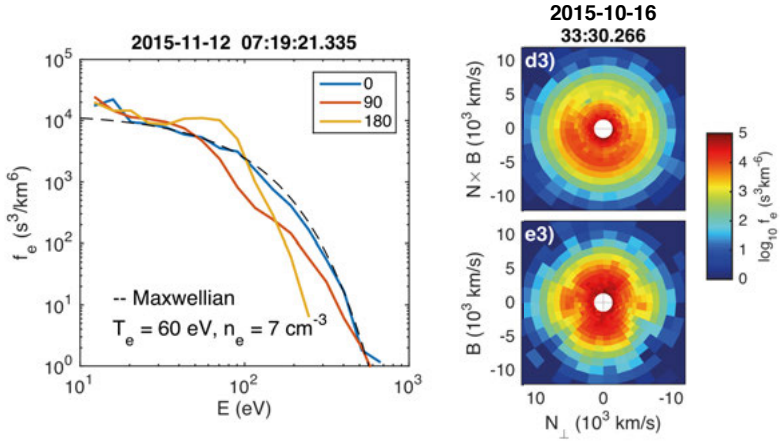

Figure 5.1. Electron phase space distributions. (left) Pitch-angle distribution showing the phase space density in the directions parallel (0°), perpendicular (90°), and antiparallel (180°) to **B**. (right) Two slices of a distribution, in the plane (top) perpendicular and (bottom) the plane containing **B**.

other effects, the phase space density will be conserved, $df/dt = 0$. However, we note that the shape of the distribution can be highly distorted. The collisionless Boltzmann equation is often referred to as the Vlasov equation, and the set of Eqs. 5.1-5.5 in addition to the Vlasov equation is often called the Vlasov-Maxwell equations.

The distribution functions found in nature are varied. Figure 5.1 shows just two examples of electron distributions, and typical ways to present them, captured by the Magnetospheric Multiscale Mission at the dayside magnetopause. To the left is a pitch-angle distribution showing distinct asymmetry between parallel and antiparallel directions, this is a typical distributions found close to open boundaries where two different plasmas mix. The dashed line is a reference Maxwellian of temperature $T_e = 60$ eV and density 7 cm^{-3} (see Eq. 5.8 below). To the right, two cuts of a distribution are shown; (top) the plane perpendicular to the ambient magnetic filed, and (bottom) a plane containing the ambient magnetic field. This distribution is both anisotropic, i.e. there is asymmetry between the parallel and the perpendicular directions, and agyrotropic, i.e. the distribution is not symmetrical around **B**, as you would expect for strongly magnetized electrons. Other features can include beams, loss cones, and flat tops, to name a few. In some cases, the distributions can be modeled as a superposition of simple distributions. One common velocity space distribution used to model a plasma is the Maxwellian distribution, which describes a plasma in thermal equilibrium:

$$f(v) = \frac{n}{\pi^{3/2} v_t^3} e^{-v^2/v_t^2}, \tag{5.8}$$

where $v_t = \sqrt{2k_BT/m}$, also known as the thermal velocity, is the velocity of a particle with mass m, and energy k_BT. In space plasma physics, it is common to use the concept of temperature even if the particle distribution is not Maxwellian. Even for an essentially collisionless plasma, the Maxwellian distribution can be a good description. In other situations, in the solar wind for example, the distributions tend to acquire a high velocity tail, which is better modeled by a so-called Kappa distribution.

The first three moments of the distribution are the density, the bulk velocity, and thermal pressure in the plasma rest frame, and are calculated as:

$$n(\mathbf{r},t) = \int_{-\infty}^{\infty} f(\mathbf{r},\mathbf{v},t)d^3v, \tag{5.9}$$

$$\langle \mathbf{v}(\mathbf{r},t)\rangle = \frac{1}{n}\int_{-\infty}^{\infty} \mathbf{v} f(\mathbf{r},\mathbf{v},t)d^3v, \tag{5.10}$$

$$\mathbf{P}(\mathbf{r},t) = m\int_{-\infty}^{\infty} (\mathbf{v}-\langle\mathbf{v}\rangle)(\mathbf{v}-\langle\mathbf{v}\rangle) f(\mathbf{r},\mathbf{v},t)d^3v. \tag{5.11}$$

These are all macroscopic quantities that describes the average properties of the plasma. To describe the evolution of these macroscopic quantities, one can calculate the first and second moments of the Vlasov equation:

$$\int_{-\infty}^{\infty} \frac{df}{dt}dv^3 = \frac{\partial n}{\partial t} + \nabla\cdot(\langle\mathbf{v}\rangle\,\mathbf{n}) \tag{5.12}$$

describing the evolution of plasma density, and

$$m\int_{-\infty}^{\infty} \mathbf{v}\frac{df}{dt}dv^3 = nm\frac{d\langle\mathbf{v}\rangle}{dt} - nq(\mathbf{E}+\langle\mathbf{v}\rangle\times\mathbf{B}) + \nabla\cdot\mathbf{P}, \tag{5.13}$$

describing the evolution of momentum. In absence of collision or other effects such that $df/dt = 0$, both the density and momentum is conserved. To close the set of equations without making use of the third moment of the Vlasov equation, which is the energy equation, we need an equation of state for the pressure $\mathbf{P}$. The equation of state can take many forms [5], but is in many cases approximated by the ideal gas law for the parallel $p_\parallel = nk_BT_\parallel$, and perpendicular $p_\perp = nk_BT_\perp$ pressures, respectively. These are the fluid equations of a plasma, and are a good description when the thermal spread in velocities is less than any other velocities involved. Every species of the plasma can be described by its own set of fluid equations.

In the fluid description an additional drift – additional with respect to the guiding center drifts for a single particle – arises due to the pressure gradients perpendicular to the magnetic field. It is called the diamagnetic drift and given by:

$$\mathbf{v}_{D,s} = -\frac{\nabla p\times\mathbf{B}}{q_s nB^2}. \tag{5.14}$$

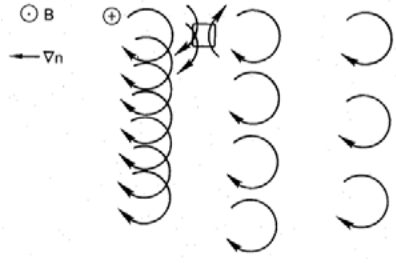

Figure 5.2. Illustration of the diamagnetic drift for positive ions. In this case the drift is due to a density gradient. Image adapted from reference [22].

In this case, there is no net motion of any one particle. It is instead the accumulated effect of the individual particles gyro motions that give a net effect, see Fig. 5.2. This can be either due to a larger number of particles on one side (this is the case shown in Fig. 5.2), or due to a higher gyro velocity of particles (equivalent to higher temperature). Since this drift is in opposite directions for electrons and ions, it is associated with a net current. This drift is often present at plasma boundaries which separate plasmas of different densities and/or temperatures.

At low frequencies, when ions and electrons respond in a similar manner to electromagnetic perturbations, the plasma can be described as a single fluid. By adding the momentum equations for two different species, for example electrons and protons, we get

$$nm\frac{d\mathbf{v}}{dt} = nq\left(\mathbf{E}+\mathbf{j}\times\mathbf{B}\right) - \nabla\cdot\mathbf{P} = 0, \tag{5.15}$$

where $\mathbf{v} = (m_e\mathbf{v}_e + m_p\mathbf{v}_p)/(m_e+m_p) \approx (m_e/m_p)\mathbf{v}_e + \mathbf{v_p} \approx \mathbf{v_p}$ is now the center of mass velocity, and $m = m_e + m_i$ is the total mass, where we have assumed charge neutrality $n_e = n_p = n$. This is the magnetohydrodynamic (MHD) description of a plasma[1] [2].

5.1 Magnetic field in a plasma

Many plasma can be described as a single conducting fluid, with conductivity σ. The conductivity is a macroscopic measure of how efficiently the assembly of particles are accelerated – or resists acceleration – by acting forces, in this case due to the electric and magnetic fields. The current are thus related to the electric and magnetic fields through Ohm's law,

$$\mathbf{J} = \sigma(\mathbf{E}+\mathbf{v}\times\mathbf{B}). \tag{5.16}$$

[1] ... for which Hannes Alfvén received the Nobel prize in physics 1970.

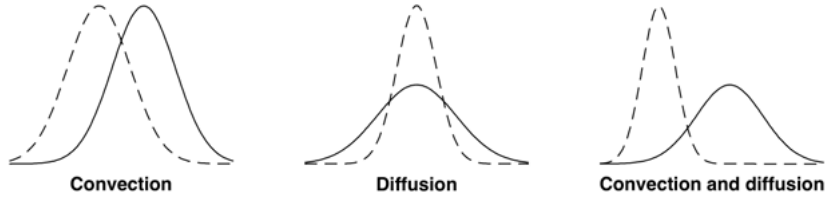

Figure 5.3. Magnetic field convection and diffusion. Dashed and solid lines show initial and subsequent magnetic field amplitudes, respectively.

By neglecting the displacement current in Ampère's law (5.4), Faraday's law (5.3), which describes the magnetic field evolution, can be written as [82, 85, 70, 90]

$$\frac{\partial \mathbf{B}}{\partial t} = \nabla \times (\mathbf{v} \times \mathbf{B}) + \frac{1}{\mu_0 \sigma} \nabla^2 \mathbf{B}. \tag{5.17}$$

The first term on the right hand side describes the convection of the magnetic field with the plasma moving at velocity $\mathbf{v}$. If L is the characteristic length scale of the plasma, and U is the characteristic velocity of the plasma perpendicular to the magnetic field, then the convection term can be written roughly as $\mathbf{B}/\mu_0 \sigma L^2$. The second term in Eq. 5.17 describes the diffusion of the magnetic field across the plasma and can similarly be written as $\mathbf{B}/\mu_0 \sigma L^2$, where $\mu_0 \sigma L^2$ has the dimension time and is often referred to as the diffusion time, τ_D. If $\tau_D \ll L/U$, the diffusion term dominates and the magnetic field tends to diffuse across the plasma and smooth out inhomogeneities, $B = B_0 e^{-t/\tau_D}$. If instead $\tau_D \gg L/U$, then the convection term dominates. In this case the magnetic field will keep its profile, but it will be translated with the same velocity as the plasma – the magnetic field is said to be *frozen in* to the plasma. An equivalent condition can be written as

$$\mathbf{E} = -\mathbf{v} \times \mathbf{B}. \tag{5.18}$$

An important consequence of this is that plasma of different origins permeated by different magnetic fields can touch by forming a boundary, but cannot be mixed [82]. The solar wind is a typical example of a plasma where the magnetic field is frozen in: the magnetic diffusion time of the solar wind is $\tau_D \approx 8 \times 10^{14}$ days while it typical takes the plasma in the solar wind 3.5 days to reach Earth.

We also note that in this picture there is no electric field component parallel to the magnetic field. Due to the high mobility of the particles, no parallel electric field has the time to establish itself during any longer times before it is short circuited by the moving particles. To break the frozen-in condition, Ohm's law (Eq. 5.16) has to be modified, or some additional resistivity other

than the classical resistivity, based on Coulomb collisions, has to be provided [84, 106].

6. Waves and instabilities

Waves are oscillating disturbances that can propagate and transfer energy and information without transferring mass. In a collisionless plasma, they are important for heating and accelerating particles. Through wave-particle interactions, they can provide so-called anomalous resistivity [84, 106], which is important since the resistivity due to plasma-neutral or Coulomb collisions is often absent. As waves are very sensitive to plasma conditions, they can also be used as a diagnostic tool to probe the plasma [109, 112]. Plasma waves can be studied using both the fluid and kinetic description of a plasma, and is reviewed in many textbooks [100, 99, 50, 22].

If a plasma is uniform and homogeneous, the electric and magnetic fields may be represented by a sum of plane waves, or what is equivalent, assume that:

$$\mathbf{E} = \mathbf{E_1}(\omega, \mathbf{k}) e^{-i(\omega t - \mathbf{k}\cdot\mathbf{x})} \tag{6.1}$$

$$\mathbf{B} = \mathbf{B_0} + \mathbf{B_1}(\omega, \mathbf{k}) e^{-i(\omega t - \mathbf{k}\cdot\mathbf{x})} \tag{6.2}$$

where ω is the frequency, $\mathbf{k}$ is the wavenumber of the wave, and $\mathbf{B_0}$ is a static magnetic field. Generally, $\omega = \omega_r + i\gamma$, is a complex number, where ω_r is the real frequency and γ is the growth rate of the wave. If $\gamma > 0$, the wave amplitude will grow in time, and if $\gamma < 0$, the wave amplitude will decay in time. A point of constant phase of the wave is traveling with the phase velocity:

$$v_{ph} = \frac{\omega}{k}. \tag{6.3}$$

The group velocity given by

$$v_g = \frac{\partial \omega}{\partial k} \tag{6.4}$$

is the velocity with which wave packets, and energy travels.

6.1 Wave-particle interactions

The Vlasov-Maxwell equations are a nonlinear system of equations describing the evolution of the particle distribution functions in time. If the system is unstable to small perturbations, i.e. small modifications in current and/or density

leads to electromagnetic fluctuations which in turn increases the density and current perturbations, then a small element of the total phase space distribution will become highly distorted as time progresses. While the Vlasov-Maxwell equations provides a complete description, sometimes it is more convenient to examine the evolution of the average quantities of $f(\mathbf{r},\mathbf{v},t)$. This can be done by dividing $f(\mathbf{r},\mathbf{v},t)$ and the electromagnetic fields into an average and a fluctuating part

$$f = \langle f \rangle + \delta f, \;\; \mathbf{E} = \langle \mathbf{E} \rangle + \delta \mathbf{E}, \;\; \text{and} \;\; \mathbf{B} = \langle \mathbf{B} \rangle + \delta \mathbf{B}. \tag{6.5}$$

The averaging should be done over a spatial scale which includes several periods of the oscillating quantities, such that

$$\langle \delta f \rangle = \langle \delta \mathbf{E} \rangle = \langle \delta \mathbf{B} \rangle = 0 \tag{6.6}$$

while

$$\langle \langle f \rangle \rangle = \langle f \rangle \qquad \langle \langle \mathbf{E} \rangle \rangle = \langle \mathbf{E} \rangle \qquad \langle \langle \mathbf{B} \rangle \rangle = \langle \mathbf{B} \rangle . \tag{6.7}$$

Making use of Eqs. 6.5 - 6.7, the averaged Vlasov equation can be written as

$$\frac{d \langle f \rangle}{dt} = \left(\frac{\partial f_s}{\partial t} \right)_{an} \tag{6.8}$$

where

$$\frac{d \langle f \rangle}{dt} = \frac{\partial \langle f \rangle}{\partial t} + (\mathbf{v} \cdot \nabla) \langle f \rangle + \frac{q_s}{m_s} [\langle \mathbf{E} \rangle + \mathbf{v} \times \langle \mathbf{B} \rangle] \cdot \frac{\partial}{\partial \mathbf{v}} \langle f \rangle \tag{6.9}$$

and

$$\left(\frac{\partial f_s}{\partial t} \right)_{an} = - \frac{q_s}{m_s} \left\langle [\delta \mathbf{E} + \mathbf{v} \times \delta \mathbf{B}] \cdot \frac{\partial}{\partial \mathbf{v}} \delta f \right\rangle . \tag{6.10}$$

Eq. 6.8 thus describes the macroscopic evolution of the distribution function due to wave-particle interactions described by Eq. 6.10. The wave-particle interactions have similar effects as plasma-neutral or Coulomb collisions. As the wave-particles interactions provide a mean to change the average properties of the distribution function in collisionless plasmas, it is often said to provide anomalous resistivity.

6.2 Lower hybrid waves

The lower hybrid drift waves are strong amplitude plasma waves that are often excited within boundaries. Despite extensive theoretical investigations since the 1960's [71, 31], coupled with observations [60, 16, 108, 4] and simulations [29, 30, 14, 25, 73], their role in different plasma remains unclear.

The lower hybrid waves are generated around the lower hybrid frequency [100]:

$$\omega_{LH}^2 = \frac{\omega_{ce}\omega_{ci}}{1+\omega_{ce}^2/\omega_{pe}^2} \ . \tag{6.11}$$

In the outer magnetosphere, both in the plasma sheet boundary layer and the magnetopause, $\omega_{pe} \gg \omega_{ce}$, and the lower hybrid frequency is reduced to $\omega_{LH} = \sqrt{\omega_{ce}\omega_{ci}}$. We can investigate the particle motion by inserting the lower hybrid frequency into the equation of motion, with $\mathbf{B} = B\hat{\mathbf{z}}$ and $\mathbf{E} = E_x\hat{\mathbf{x}}$. By neglecting terms of order $\sqrt{m_e/m_i}$, we obtain:

$$0 = -\frac{eE_x}{m_e}\hat{\mathbf{x}} - \omega_{ce}\mathbf{v}\times\hat{\mathbf{z}} \quad \text{(electrons)} \tag{6.12}$$

$$-i\omega_{LH}\mathbf{v} = \frac{eE_x}{m_i}\hat{\mathbf{x}} \quad \text{(ions)}. \tag{6.13}$$

The electrons are magnetized and follow the motion $\mathbf{v}_e = \hat{\mathbf{y}}eE_x/m_i\omega_{ci}$, perpendicular to both the magnetic and electric fields. The ions are unmagnetized and oscillate in the electric field direction according to: $\mathbf{v}_i = \hat{\mathbf{x}}eiE_x/m_i\omega_{LH}$, 90° out of phase with the electrons. When taking into account terms of order $\sqrt{m_e/m_i}$, the particle trajectories become elongated orbits. Also, we should in practice also consider a small oscillating electric field component parallel to the magnetic field, causing the electrons to move rapidly along the magnetic field. The lower hybrid waves are important as mediators between the slowly moving ions and rapidly moving electrons, as well as between the directions parallel and perpendicular to the magnetic field.

6.3 The lower hybrid drift instability

The lower hybrid drift instability [71, 31, 60] is a cross field current-driven instability, which has been identified both in laboratory [16] and space [60]. The free energy which supports the instability comes from the cross field current and inhomogeneities in the plasma. It was early suggested that the instability could be associated with anomalous resistivity [31, 59, 93], and play a significant role in the development of magnetic reconnection [106]. The perhaps simplest plasma configuration for the lower hybrid drift instability consists of a density inhomogeneity perpendicular to the background magnetic field, giving rise to cross field diamagnetic drifts of electrons and ions, see Fig. 6.1. In a more general case, gradients in both the temperature and magnetic field also have to be taken into account. The propagation direction of the unstable wave is both perpendicular to the magnetic field, $\mathbf{k}\cdot\mathbf{B} \approx 0$, and the pressure gradient direction, $\mathbf{k}\cdot\nabla p \approx 0$.

Yoon [115] derives a dispersion relation for unmagnetized ions and magnetized electrons, which in the case of no guide field, $\mathbf{B} = B(z)\hat{\mathbf{x}}$, and $n = n(z)$,

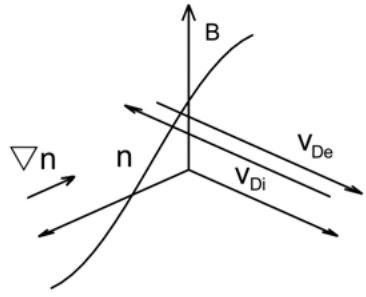

Figure 6.1. Simple inhomogeneous plasma configuration.

becomes:

$$0 = 1 - \frac{\omega_{pi}^2}{k^2 v_{ti}^2} Z' \left(\frac{\omega - k_y V_{Di}}{k v_{ti}} \right) + \frac{2\omega_{pe}^2}{k^2 v_{te}^2} \left(1 + \frac{\omega - k_y V_{De}}{k_x v_{te}} J_0(b) I_0(\lambda) e^{-\lambda} Z(\xi) \right) \tag{6.14}$$

where Z is the plasma dispersion function [41], J_0 is the Bessel function of the first kind of order 0, I_0 is the modified Bessel function of the first kind of order 0, and the dimensionless variables are given by:

$$b = -\frac{k_y V_{De}}{\omega_{ce}} \qquad \lambda = \frac{k_y^2 v_{te}^2}{2\omega_{ce}^2} \qquad \xi = \frac{\omega}{k_x v_{te}}. \tag{6.15}$$

The solutions to the dispersion relation (6.14) are found numerically, and for parameters relevant for the event in Paper I, it is plotted in Fig. 6.2. The growth rate peaks at $k\rho_e \gtrsim 1$, with the real frequency slightly below the lower hybrid frequency, $\omega_r \sim \omega_{LH}$, and the growth rate, $\gamma \lesssim \omega_{LH}$. A thin current sheet is equivalent to strong gradients, or equivalently, small gradient length scales, for example the density gradient length scale: $L_n \equiv \left(\frac{1}{n}\frac{dn}{dx}\right)^{-1}$. Decreasing L_n from $0.5\rho_i$ to $0.3\rho_i$ gives rise to stronger cross field drifts that in this case doubles the growth rate. Observations of lower hybrid drift waves are discussed in Paper I.

6.4 The Buneman instability

One instability, which is often invoked when it comes to explaining the generation of slow electron holes [67, 21], such as we observe them in Paper II, is the Buneman instability [10].

In the cold plasma limit, where we consider all the particles of any population to move with the same velocity, the Buneman instability has the following dispersion relation:

$$1 - \frac{\omega_{pi}^2}{\omega^2} - \frac{\omega_{pe}^2}{(k v_b - \omega)^2} = 0. \tag{6.16}$$

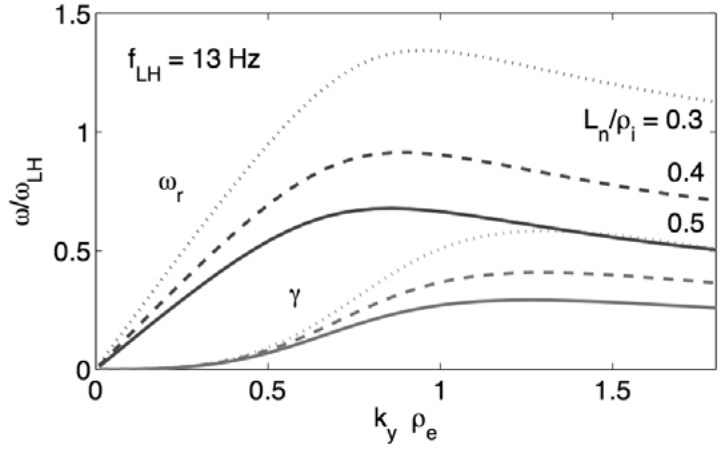

Figure 6.2. Dispersion relation for lower hybrid drift waves [115]. The parameters are $L_n = [0.3\ 0.4\ 0.5]\rho_i$, $T_e = 2000$ eV, $T_i = 3000$ eV, $B_0 = 20$ nT and $n = 0.08$ cc. The growth rate peaks at $k\rho_e \gtrsim 1$, with $\omega_{LH} \sim \omega_{LH}$ and $\gamma \lesssim \omega_{LH}$.

This expression includes two plasma populations, stationary ions and electrons that drift with the velocity v_b. In the slow phase velocity limit, where $\omega \ll \omega_{pi}$, this reduces to

$$kv_b = \omega + \omega_{pi} + \frac{\omega_{pe}\omega_{pi}^2}{2\omega^2}. \tag{6.17}$$

By inserting the complex frequency, $\omega = \omega_r + i\gamma$, into (6.17), we obtain the real frequency at maximum growth rate:

$$\omega_r = \left(\frac{\omega_{pe}\omega_{pi}^2}{16}\right)^{1/3}, \gamma = \sqrt{3}\omega_r, \tag{6.18}$$

for $kv_b = \omega_{pe}$, see Fig. 6.3. We can note a significant growth rate for a quite wide range of real frequencies where a higher frequency (or correspondingly a higher $kv_b - \omega_{pe}$) gives a higher ratio of v_{ph}/v_b and vice versa. The phase velocity of the wave with maximum growth rate is

$$v_{ph} = \frac{\omega_r}{\omega_{pe}/v_b} = \left(\frac{m_e}{16m_p}\right)^{1/3} v_b \approx 0.03v_b. \tag{6.19}$$

If the wave grows up to the point when it starts to trap the drifting electrons, the subsequently generated electron holes are thus generated at v_{ph}, a phase velocity which corresponds to a fraction of the relative drift velocity of the ions and electrons. For a plasma with vanishing temperatures, this instability can easily be driven unstable. A plasma, however, can in general not be considered cold, and resonant interaction with the thermal populations can lead to linear

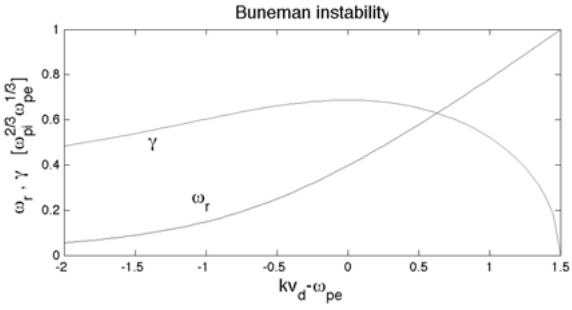

Figure 6.3. The complex frequency of the Buneman instability in the cold plasma limit with one stationary ion population and one drifting electron population. There is a significant growth rate for a range of real frequencies.

damping of the wave. The critical drift velocity as derived by Buneman (for $T_e = T_i$) for the electrons is $0.9v_{te}$, where v_{te} is the thermal velocity of the electron population. This required drift is large, and is not observed in nature.

In space, electron beams with large drift speeds are often observed together with a hot background with relatively small or zero drift speed. For an unmagnetized plasma, or propagation parallel to the ambient magnetic field, the dispersion relation is given by

$$0 = 1 - \frac{\omega_{pi}^2}{k^2 v_{ti}^2} Z'\left(\frac{\omega}{k v_{ti}}\right) - \frac{\omega_{pe,bg}^2}{k^2 v_{te,bg}^2} Z'\left(\frac{\omega}{k v_{te,bg}}\right) - \frac{\omega_{pe,beam}^2}{k^2 v_{te,beam}^2} Z'\left(\frac{\omega - k v_{beam}}{k v_{te,beam}}\right), \tag{6.20}$$

where Z is the plasma dispersion function [41], $v_{ts} = \sqrt{2k_B T_s/m_s}$ is the thermal speed and $\omega_{ps} = \sqrt{n_s e^2/\varepsilon_0 m_s}$ is the plasma frequency of population s and v_{beam} is the electron beam speed. Figure 6.4 demonstrates the solution to the dispersion relation for two different plasma configurations, only differing in the drift speed of the electron beam v_{beam}. When the beam speed is sufficiently low, an ion-electron instability is dominant, giving a phase speed well below the thermal speed of the electron background. When increasing the beam speed, an electron-electron instability becomes dominant, giving a phase speed comparable to both the thermal speed of the electron background and the beam speed, $v_{ph} \approx 0.24 v_{te,bg} = 0.5 v_{beam}$. The ion-electron instability can couple the ion and electron populations and decrease the current carried by the much faster electrons (for illustration of this see e.g. Figure 4.5). This is a form of anomalous resistivity, i.e. effective resistivity without collisions. The electron-electron instability will have smaller effect on the current. This is investigated in Paper III.

(a) Ion-electron instability (b) Electron-electron instability

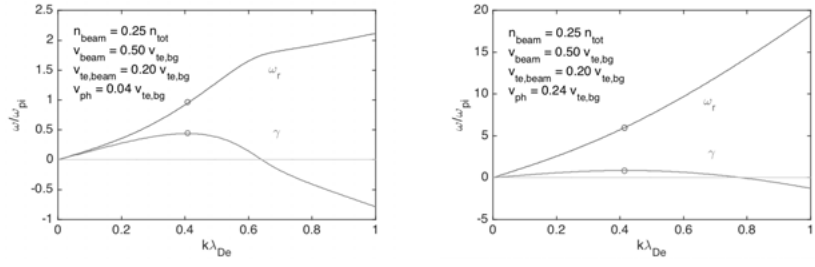

Figure 6.4. The dispersion of a modified Buneman instability for a plasma with three populations: thermal ions, a thermal electron background, and cold electron beam. The parameters are given by $T_i = T_{e,bg} = 25T_{e,beam}$, $n_{e,beam} = 0.25(n_{e,bg} + n_{e,beam}) = 0.25n_i$, λ_{De} is based on the electron background parameters, and v_{ph} is given for the wavenumber corresponding to the highest growth rate γ. Only the beam speeds differ and are given by (a) $v_{e,beam} = 0.5v_{te,bg}$, and (b) $v_{e,beam} = 0.7v_{te,bg}$.

7. Boundary layers

Thin extended regions often form at boundaries between plasma of different character. Processes at these boundaries determine when and how the separated plasmas mix, and can therefore have large scale implications. For example, the Sun-Earth interaction is largely dependent on the micro physics of the dayside magnetopause down to electron scales, and one of the major problems in certain types of fusion devices regards the confinement of the plasma.

In this chapter, we give a brief introduction to what kind of boundaries can form, and processes which will cause boundaries to break down.

7.1 Discontinuities

A boundary is by definition accompanied by changes in plasma parameters. In the simplest case they are modeled as infinitely thin, where the changes occur as discontinuities. Figure 7.1 depicts a few type of discontinuities that occur in a plasma modeled as a single fluid (MHD). The bowshock can be both a slow and fast shock, and is typically quasi-parallel (shock normal angles $\theta_B < 45^\circ$) on the dusk side and quasi-perpendicular ($\theta_B > 45^\circ$) on the dawnside of Earth. A tangential discontinuity has no normal magnetic field $\hat{\mathbf{n}} \cdot \mathbf{B} = 0$, and will thus allow no plasma to cross if the magnetic field is frozen-in to the plasma. This is typically how a closed boundary is configured. By allowing a finite normal component of the magnetic field B_n and velocity v_n, the two sides of the boundary become connected. If B_n and v_n are continuous across the boundary, the boundary can be shown to obey the jump condition

$$\Delta \mathbf{v_t} = \frac{\Delta \mathbf{B_t}}{\sqrt{nm\mu_0}}, \tag{7.1}$$

in the tangential velocity $\mathbf{v_t}$ and magnetic field $\mathbf{B_t}$ where Δ signifies the asymptotic jump in the parameters [5]. As the tangential electric field also has to be constant across the boundary, $\Delta \mathbf{v_t}$ and $\Delta \mathbf{B_t}$ are coplanar, but are scaled with the normal components

$$\Delta \mathbf{v_t} \quad = \quad \frac{v_n}{B_n} \Delta \mathbf{B_t}, \tag{7.2}$$

again showing that the tangential velocities will experience a jump across the boundary. Finding tangential plasma flows that can be described by Eq. 7.1

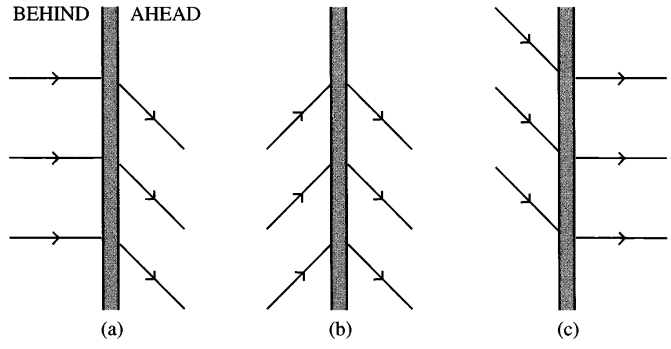

Figure 7.1. Different kind of magnetic field geometries at discontinuities (a) Slow shock. (b) Alfvén wave, or rotational discontinuity (c) Fast shock. Image adapted from Priest and Forbes (2000) [90].

and Eq. 7.2 is often a good indication that a boundary is rotational and is commonly used to identify reconnection jets at the magnetopause [97, 94, 105].

The MHD description can well describe the large scale properties of discontinuities. At small scales however, the electrons and ions will behave differently and additional descriptions are necessary. In the next section, we will describe the process of reconnection, which is intimately related to thin boundaries and is responsible for changing magnetic field topology.

7.2 Magnetic reconnection

Magnetic reconnection [8, 90] is a process whereby the magnetic topology is changed, and energy stored in the magnetic field is transferred to particle energy. Around Earth, it is believed to be responsible for the transport of plasma across the Earth's magnetopause but also for major energy conversion and particle acceleration in the magnetotail [98]. It is also believed to be important for heating of the coronae of stars [17], for coronal mass ejections [33], for supersonic winds of accretion discs [47], and for acceleration of cosmic rays [34].

While the net magnetic flux crossing the surface of any volume has to be zero, Faraday's law describes rotation of the magnetic field, which may result in a change in connectivity of the magnetic field (Figure 7.2). A change in connectivity has occurred if two particles that were initially on the same field line end up on different field lines. The magnetic field must thus rotate relative to the plasma. This can happen if the magnetic field frozen-in condition is broken: $\mathbf{E} + \mathbf{v} \times \mathbf{B} \neq 0$. This condition is broken inside the so-called diffusion region which is different for electron and ions. In a 2D magnetic field configuration, $\mathbf{B} = B_x\hat{\mathbf{x}} + B_y\hat{\mathbf{y}}$, this can occur if there is an electric field

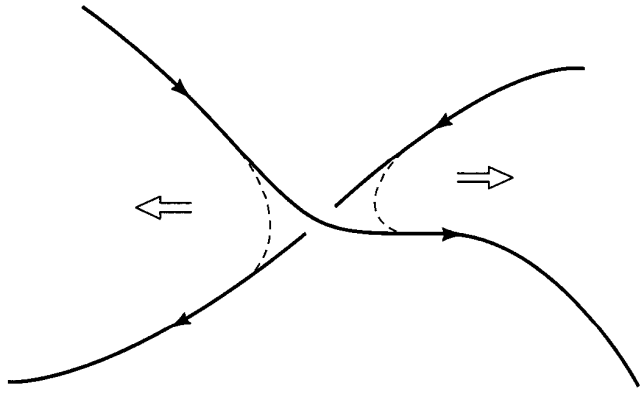

Figure 7.2. Change of connectivity of magnetic field lines. Image adapted from Biskamp (2000) [8].

normal to the plane $\mathbf{E} = E_{rec}\hat{\mathbf{z}}$ inside the diffusion region. In a 3D magnetic field configuration which is the most common case in nature, the most general condition is that the closed line integral of the parallel electric field has to be non-vanishing

$$\int E_{||} ds \neq 0, \tag{7.3}$$

where the integration is done along a set of field lines inside the diffusion region.

A local change in magnetic topology can lead to a global change of magnetic field configuration. The Lorentz force for a single fluid MHD plasma can be written as

$$\mathbf{j} \times \mathbf{B} = -\mu^{-1} \nabla \cdot \left(\frac{1}{2} B^2 \mathbf{I} + \mathbf{B}\mathbf{B} \right). \tag{7.4}$$

There is thus one part that represents the magnetic pressure, and one part which depends on the parallel gradient of $\mathbf{B}$: $\nabla \cdot (\mathbf{B}\mathbf{B}) = \mathbf{B} \cdot \nabla \mathbf{B}$, representing the magnetic tension. Figure 7.3a shows the direction of the two terms for an equilibrium magnetic field configuration. The magnetic tension acting to straighten the field lines is balanced by the magnetic pressure which is larger at the edges and vanishing at the center. Figure 7.3b shows a similar but stretched out magnetic configuration. Given the same boundary conditions, the magnetic pressure in the stretched out regions is now increased while the curvature and magnetic tension is decreased. The opposite is true for the compressed regions at the top and bottom. The resultant force will thus be to push the magnetic field lines in at the left and right side, and push them out at the top and bottom. The extreme case of a stretched out magnetic field configuration is two adjacent regions with antiparallel fields. This is what typically

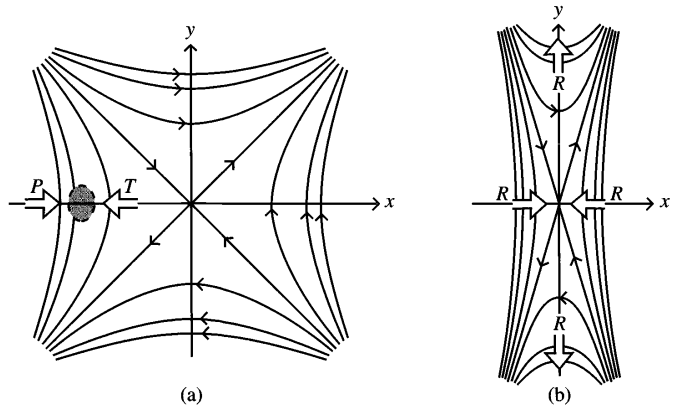

Figure 7.3. Equilibrium and non-equilibrium magnetic field configuration. P indicates the magnetic pressure and T the magnetic tension. R is the resultant force due to P and T. Image adapted from Priest and Forbes (2000) [90].

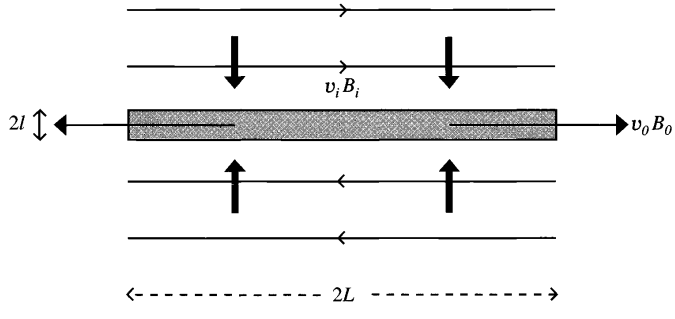

Figure 7.4. Basic set up of the Sweet-Parker reconnection model. Image adapted from Priest and Forbes (2000) [90].

happens at the nightside of Earth, where the field lines convecting from the dayside are dragged out by the plasma and form the elongated magnetotail. If the tension can be released, it will accelerate the plasma, thus transforming magnetic field energy to particle energy.

There are many models that describe magnetic reconnection in different regimes, but there is not yet a unified theory. One of the first to make predictions for 2D reconnection in a time-stationary resistive current sheet was Parker [86], extending upon the work by Sweet [101], and before that Giovanelli [46]. The basic idea was that added magnetic flux will be convected towards the center of the current sheet with the plasma, where the finite resistivity will cause the magnetic field to diffuse across the plasma and be ejected. A time-stationary situation is attained when the added flux is balanced by the ejected flux. The equilibrium will thus depend on the plasma resistivity. A

sketch of the configuration is shown in Figure 7.4; $2L$ is the width and $2l$ is the thickness of the current sheet. The upstream, or inflow, parameters are denoted by the subscript 'i' while the downstream, or outflow, parameters are denoted by the subscript 'o'. Time-independence requires the out-of-plane electric field E_t to be uniform in space. The following derivation closely follows Priest and Forbes (2000) [90].

Outside the current sheet, the resistivity is negligible and the magnetic field is convected with the plasma:

$$E_t = v_i B_i. \tag{7.5}$$

Inside the current sheet, the resistivity is finite while the magnetic field is low such that

$$E_{rec} \equiv E_t = \eta\, j_{max} \simeq \eta B_i / \delta \mu_0, \tag{7.6}$$

where in the last step Ampère's law is used to estimate the current j_{max} in the center of the current sheet. Eliminating E_t gives us the relation

$$v_i = \eta / \delta \mu_0, \tag{7.7}$$

To relate the inflow parameters to the outflow parameters we use the continuity equation and the momentum equation. The conservation of mass as stated in the continuity equation leads to the relation

$$\rho_i v_i L = \rho_o v_o \delta. \tag{7.8}$$

For equal densities in the inflow and outflow region, Eqs. 7.7 and 7.8 can be combined to give the inflow speed

$$v_i^2 = \frac{\eta v_o}{\mu_0 \delta}. \tag{7.9}$$

When the plasma has reached the stagnation point (the point at the center of the region where the velocities vanish), it will be accelerated by the Lorentz force along the current sheet in the outflow direction x, $(\mathbf{j} \times \mathbf{B})_x \approx j_{max} B_2 = B_i B_o / \delta \mu_0$. By equating the Lorentz force term with the inertial term $\rho(\mathbf{v} \cdot \nabla v_x)$, neglecting the pressure, we obtain

$$\rho \frac{v_o^2}{L} \approx \frac{B_i B_o}{\mu_0 l} \tag{7.10}$$

By using the conservation of magnetic flux $\delta \cdot \mathbf{B} = 0$ that gives $B_i / \delta \approx B_2 / L$, Eq. 7.10 gives the outflow speed

$$v_o = \frac{B_i}{\sqrt{\mu_0 \rho}} \equiv v_{A,i}, \tag{7.11}$$

where $v_{A,i}$ is the Alfvén speed in the inflow region. The speed of the inflowing plasma decides the rate at which reconnection proceeds, and is often scaled with a dimensionless variable $R_{me} = Lv_{A,i}/\eta$ called the reconnection rate:

$$v_i = \frac{v_{A,i}}{R_{me}^{1/2}}. \tag{7.12}$$

In practice, the reconnection rate predicted by the Sweet-Parker model is often very small as $R_{me} \gg 1$. For example, in the stellar corona $R_{me} \sim 10^6 - 10^{12}$, the predicted reconnection speed of magnetic field lines is 10^{-3} to 10^{-6} of the Alfvén speed, which can not explain the explosive releases of energy observed in solar flares [5].

Petschek [88] later suggested that the plasma does not only cross the thin central current layer, but can also move across extended shocks emanating from a central Sweet-Parker current layer.

The next significant step was to allow for relative motion of the ions and electrons, in the Hall-MHD model [98]. By allowing the ions and electrons to have different motion, we can write Ohm's law as (see e.g. [5])

$$\begin{aligned} \frac{e}{m_e}\frac{d\mathbf{J}}{dt} &= ne\left(\mathbf{E} + \mathbf{v}_e \times \mathbf{B}\right) + \nabla \cdot \mathbf{P}_e \\ &= ne\left(\mathbf{E} + \mathbf{v}_i \times \mathbf{B}\right) - \mathbf{J} \times \mathbf{B} + \nabla \cdot \mathbf{P}_e, \end{aligned} \tag{7.13}$$

where we have omitted collisions, and the center of mass is taken to move with the ions $\mathbf{v} \approx \mathbf{v_i}$. This leads to a scenario where the ions decouple from the magnetic field in an outer region, the ion diffusion region (Figure 7.5a), while the magnetic field continues to be convected with the electrons to the edge of an inner, electron diffusion region, inside which the magnetic field ultimately diffuses across the plasma and reconnect. This gives the so called Hall current system as illustrated in Figure 7.5b. The Hall currents are associated with the Hall magnetic fields [36]. The line along which the magnetic field reconnects is called the X-line. In 2D reconnection without guide field (the finite out-of-plane magnetic field), it is the line (extending in the out-of-plane direction) at which the magnetic field vanishes. The lastly reconnected field lines extend from the X line and form the separatrices. The separatrices are thus the outer edges of reconnected plasma. Under conditions when the plasma inflow is symmetric about the X line, the Hall magnetic field has quadrupolar structures. At boundaries where the plasma density changes significantly between the two sides, as for example at the magnetopause between the magnetosheath and the magnetosphere, magnetic reconnection is asymmetric. The magnetic reconnection outflow is dominated by the higher density (e.g. magnetosheath) plasma, and the flow stagnation point is no longer co-located with the X line but is shifted toward the low-density (e.g. magnetospheric) side [18]. This leads to an asymmetric outflow pattern, and as a result, the Hall magnetic field structure is modified, becoming more dipolar than quadrupolar (Figure 7.6) [92, 102, 81, 114, 83].

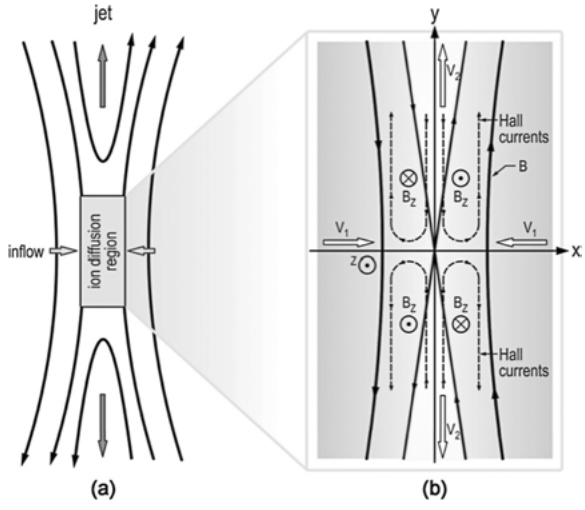

Figure 7.5. Inside the ion diffusion region, the magnetic field and ions are decoupled from the field lines while the electrons remain frozen-in. This creates the Hall current system, and associated Hall magnetic fields. Image adapted from Burch et al. (2015), with original figure from Sonnerup (1979) [98].

One unresolved question regarding magnetic reconnection in nature is what balances the reconnection electric field inside the electron diffusion region. Considering the electron dynamics only, and neglecting wave-particle interactions, the quasi-stationary electric field has to be balanced directly through the electron momentum equation. [53, 107]. Considering Faraday's law, terms contributing to the magnetic diffusion have to be rotational. As such, the diagonal terms of the electron pressure divergence are not important, and only the off-diagonal terms can contribute. Therefore, for 2D reconnection, where the magnetic field lies in the xy-plane, the reconnection electric field E_y could be supported by the following terms [53, 107]:

$$E_{rec} = E_y = -(\mathbf{v_e} \times \mathbf{B})_y - \frac{1}{ne}(\partial_x P_{e,xy} + \partial_z P_{e,yz}) - \frac{m_e}{e}(\partial_t + \mathbf{v_e} \cdot \nabla) v_{e,y}. \quad (7.14)$$

The importance of these different terms to support magnetic reconnection has been investigated thoroughly in numerical simulations (see e.g. refs. [55, 91, 52] and ref. [107] and references therein), and it has been found that both the off-diagonal electron pressure terms and the inertia term are important, in different situations (see e.g. [52, 54]).

However, numerical simulations are computationally expensive, and there is yet no single simulation which can properly represent all the temporal and spatial scales for realistic parameters. To reduce the computational cost it is common to reduce the mass ratio between ions and electrons, use 2D instead of 3D environments, and use unrealistic separation of physical scales. For ex-

ample Jara-Almonte et al. (2014) [63] showed using 2D simulations that a physical separation between the electron inertial length and the Debye length $d_e/\lambda_{De} = c/v_{the}$ lead to Debye scale turbulence in the electron diffusion region. The turbulence was caused by streaming-instabilities, and the resulting turbulence affected both the density, electrostatic potential, pressure and current structure within the electron diffusion region.

The study of these electron-scale processes has until recently only been possible in numerical simulations. After the launch of the MMS satellites in spring 2015, the detailed study of electron distributions and current systems on scales at or below the electron spatial scales has become possible. Many studies have observed agyrotropic electron distributions (see for example Figure 7.6 adapted from Paper IV) in the vicinity of the electron diffusion region [13, 12, 83, 37]. The most common agyrotropic feature consists of crescent shaped electron distributions in the plane perpendicular to the ambient magnetic field, and have been predicted in numerical simulations [52, 7]. They are attributed to finite gyroradius effects as electrons from a denser or hotter region perform partial gyroorbits into an adjacent region. These agyrotropic components of the electron population can be associated with large currents that may significantly alter the overall current structure. Figure 7.6 shows the observed electron velocities in a thin reconnecting current layer studied in Paper IV. The flow structure showed an electron outflow region (arrows pointing downwards) directly adjacent to the electron inflow (upward-inward pointing arrows to the right of the dashed line). The region of largest outflow seen between the two lines were supported by agyrotropic electron motion (Figure 7.6c-d).

Although the observations of inner reconnection regions are becoming more abundant, many questions are still outstanding. For example, what is the role of waves in facilitating magnetic reconnection.

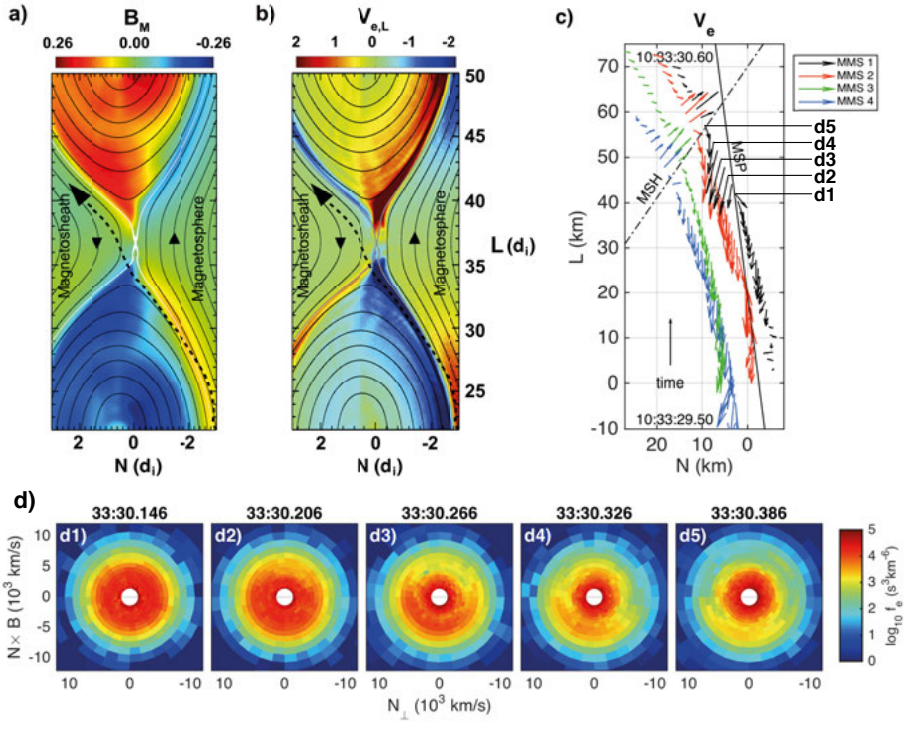

Figure 7.6. Hall magnetic field and electron flow structure inside the ion diffusion region in asymmetric magnetic reconnection. The (a) out-of-plane magnetic field B_M and (b) electron velocity component $v_{e,L}$ are from a 2D particle-in-cell simulation [23]. (c) The structure of the electron flow is consistent with a passage (dashed line in panels a and b) of the reconnection region close to the electron diffusion region. (d) Electron distributions in the plane perpendicular to the magnetic field (for the instances marked by d1-d5 in panel c) as observed by MMS1. The largest amplitude electron flows consists of agyrotropic crescent shaped distributions. Figure adapted from Paper IV.

8. Future prospects

In the footsteps of the Cluster mission, the Magnetospheric Multiscale mission has opened up a door to a new level of space physics to be explored. Already, several studies have explored regions down to scales comparable to the electron gyroradius and electron inertial length. This has been possible due to the small separation (<15 km) between the four spacecraft and the high temporal resolution of the collected data. However, the small separation between the spacecraft comes at a price: unless the motion of the spacecraft relative to your region of interest is very small, you will only observe it for a short time as the four spacecraft inevitably pass it (or close by it) in close succession. In this sense the name "Multiscale" is a misnomer, since you only have access to the small spatial, and fast temporal scales. One remedy to the problem of resolving multiple spatial and/or temporal scales is to perform conjunction studies with other spacecraft, for example the (durable) Cluster spacecraft. Another helpful tool to understand the context of your short observation is of course numerical simulations. However, at the moment, global (or at least non-local) numerical simulations of well separated multi-scale plasma processes is computationally prohibitive. Therefore, the variety and richness of space observations greatly outweighs the range of simulations to compare them to. This is truly a luxurious problem, and might in a way be its own solution.

In this thesis, we have performed two case studies using MMS data. These two events have by themselves provided new insights into electron dynamics in thin reconnecting current sheets, but still only constitutes a minuscule subset of current sheet configurations and stages of evolution. One of the major questions regarding magnetic reconnection is in fact how the process is initiated, and this is a question that has not yet been addresses with MMS. It is admittedly a hard question, how can you know it is the onset of reconnection if you can not catch the temporal evolution properly. To address this question properly, it is important to systematically study current sheets with a wide range of properties (both boring and exciting). This is something that is possible with MMS, and would provide a great contribution to magnetic reconnection research.

So, after having spent two paragraphs to say we need to make comparative studies of thin current sheets in order to solve the outstanding questions regarding magnetic reconnection, the next question immediately follows, *and then*[1]? Well, magnetic fields permeates at least the local Universe, and plasma

[1] Well, after some consideration it turned out we had misunderstood the entire thing, so now we have to send up eight, no wait, twelve (!) spacecraft...

constitutes the major part of the observable Universe. But to start close at home, many missions to our outer planets has been purely exploratory with brief flybys providing the only in situ measurements[2]. At the same time, the magnetospheres of the outer planets are diverse plasma environments – there are discs and dust, strong magnetic fields and significant quadrupole moments, a severely tilted dipole axis, bowshocks, and radiation belts – that may provide looking glasses into astrophysical processes[3]. The rings of Saturn for example are often compared to protoplanetary discs. Another fundamental plasma process that, like magnetic reconnection, is not fully understood is turbulence. Plasma turbulence is thought to play a major role in heating and accelerating particles throughout the Universe, for example in supernova remnants. Both magnetic reconnection and turbulence can also have large effects in plasma laboratories. They can for example have detrimental effects on the confinement of plasma in fusion devices. If the progress in understanding fundamental plasma processes provided by space research will someday aid in facilitating plasma fusion, that would be a treat.

[2]The only orbiters are Galileo, Juno, and upcoming JUICE at Jupiter, and Cassini at Saturn.
[3]The stars are not the limits!

9. Acknowledgments

Det är många jag skulle vilja tacka, utan att veta hur. Så jag tänkte mestadels gå efter devisen, ingen nämnd, ingen glömd! Vi börjar med lite engelska.

Cluster: I suppose it's impossible to mention everybody that should be mentioned. It's just really simple, without the hard work that everyone involved in Cluster ($\times 2$) put in, where would we be today[1]? Great thanks to all the people that has been working with Cluster throughout the years, and in particular EFW, FGM, STAFF, CIS and PEACE teams!

MMS: I'm pretty happy that my PhD studies extended into the MMS age[2]. Thanks to all the MMS teams that work so hard to give the best to the community.[3]

Och så de mindre viktiga...

Mats Du ställer frågor tills man börjar ställa dem till sig själv, och undrar vad man egentligen håller på med, och varför, på ett bra sätt. Du har lärt mig ett och annat om hur det är att vara forskare, men framför allt vill jag tacka dig för allt tålamod och värme du visat mig genom åren, blandat med humor och vishet[4]. Det känns som om du alltid sett till mig som person i första hand, och det är jag tacksam för.

Andris och Yuri Duktiga forskare till trots[5], er kommer jag att sakna för att ni skrattar så lätt...

Daniel Min yngre kollega och personlige forskningscoach!

Röta Alla ni som spelat pingis med mig! Du som (typ) styrt mig mot horisonten och vattnat mina blommor! Du som förser mig med te och chips och vin! Ni som löst korsord och druckit te med mig! Ni som aldrig spelade paintball med mig! Ni som man blir glad av varje gång man ser! Du som sällan lagar mat till mig! Ni som aldrig ger upp med att bjuda med oss rymdfysiker! Ni som har lätt till skratt! Ni gröngölingar som har framtiden för er! Ni som förslösar er tid på viktiga dataspel! Du som gillar pussel! Du som spelar gitarr! Du som gör världen bättre! Alla mina förebilder! Ni som kom med till Åre! Och alla ni klättrare!

[1] At the magnetospheric [if you're good at epochs, insert something suitable here]?

[2] That's how it feels like to me, a new age...

[3] I honestly spent way too much time to find the proper superlatives... When I think about all the preparation, all the ever ongoing calibration, all those SITL hours.

[4] Jag tar inte i för mycket nu va?

[5] Sviker min svenska mig..?

Familjen Som man inte ens behöver nämna...[6][7]

[6]Fast nu gjorde jag det ändå...
[7]Och de fick en helt egen sida... :)

10. Summary of papers

Here follows a short summary of all papers included in the thesis, together with a description of the contribution made by the author of this thesis to each publication.

Paper I

Lower hybrid drift waves: Space observations
Phys. Rev. Lett., 109, 55001, doi:10.1103/PhysRevLett.109.055001.

Lower hybrid waves are primarily electrostatic waves polarized in the plane perpendicular to the ambient magnetic field $\mathbf{B_0}$, and have a characteristic scale of $k\rho_e \approx 1$. In this paper we studied an event when two of the four Cluster satellites was located close together in the plasma sheet boundary layer and operated in burst mode. The separation between the spacecraft was on the order of the electron gyroradius, which allowed us to make the first unambiguous measurements of lower hybrid drift waves, including phase velocity, wavelength, and electrostatic potental. We found that the electric wave $\delta\mathbf{E}$ field was associated with a wave magntic field due to the current carried by electrons due to their guiding center drift: $\mathbf{v}_{E\times B} = \delta\mathbf{E} \times \mathbf{B_0}/B_0^2$. This discovery lead to a method to determine the wave phase velocity using a single spacecraft, making the study of lower hybrid waves much more viable. The method has been used in several studies since [61, 49, 68, 32].

My contribution: I performed the data analysis and lead the writing of the paper.

Paper II

Slow electron phase space holes: Magnetotail observations
Geophys. Res. Lett., 42, doi:10.1002/2015GL063218.

Electrostatic solitary waves are nonlinear plasma waves associated with dipolar electric fields and are commonly observed in both space and laboratories. They can be excited through field-aligned streaming instabilities and are often signs of nearby energetic processes that can accelerate plasma into beams. The large amplitude electric fields can lead to trapping of electrons and

ions, which may significantly alter the particle distributions and create holes in phase space. Due to their small field-aligned scale (typically 10 electron intertial lengths), they have been diffiucult to study in detail. In this paper, we perform cross-spaceraft measurements of electrosatic solitary waves in the plasma sheet boundary layer (the same crossing as in Paper I). We could thus make the first unambiguous measurements of phase speed, length, and electrostatic potential of these waves in space. Since the waves were observed by two spacecraft, they were inferred to have divergent electric fields, consistent with electron phase space holes. The phase speed was comparable to the ion thermal speed, suggesting the instability leading to their formation involved both electrons and ions. This is an important class of instabilities, as ion-electron coupling can lead to effective resistivity and current reduction.

My contribution: I planned the study, performed the data analysis and lead the writing of the paper.

Paper III

Slow electron holes in multicomponent plasmas
Geophys. Res. Lett., 42, doi:10.1002/2015GL065390.

The study in Paper II lead us to ask the question, under what conditions is the ion-electron streaming instability dominant? The classical two-stream instability involves the bulk motion of two plasma populations well separated in phase space. Marginal conditions for the ion-electron streaming instability with finite temperatures $T_e = T_i$ requires that the electron bulk drift speed exceeds the electron thermal speed, something that is rarely observed in space, where the electrons often have a large thermal background in addition to any beams. In this paper we investigate the paramteter space of streaming instabilities with three plasma components; thermal non-drifting ions, thermal non-drifting electrons and relatively cold drifting electrons. At high drift speeds, the thermal electrons interact with the electron beam, generating waves at phase speeds comparable to the electron beam speed. At lower drift speeds, the electron-electron instability is marginally stable, and will allow for a modified ion-electron instability to evolve. This prediction was compared to data from the dayside magnetopause [48]. By performing the instability analysis based on observed particle data, it was found that by decreasing the beam temperature – to simulate the pre-instability conditions – slow waves with phase speed comparable to measured phase speeds could be driven unstable.

My contribution: I planned the study and performed the dispersion relation analysis and lead the writing of the paper. Daniel Graham made essential contributions by performing the analysis of space data.

Paper IV

Finite gyroradius effects in the electron outflow of asymmetric magnetic reconnection

Geophys. Res. Lett., 43, doi:10.1002/2016GL069205.

The inner region of magnetic reconnection, called the electron diffusion region, is associated with thin current sheets where gradients in the magnetic field and plasma is comparable to the electron gyroradius. The dynamics of electrons within this thin region is thought to be important in the onset and evolution of magnetic reconnection, and can therefore have implicaitons for large scale physics. Before the launch in 2015 of the Multiscale Magnetosperic (MMS) mission, it could not be well studied due to instrumental limitations, and is therefore yet little understood. In this paper, we use data from the four MMS satellites to study the spatial structure and electron distributions in an electron-scale current sheet close to the electron diffusion region. In the electron outflow near the X line, all four MMS spacecraft observe highly structured electron distributions in a region comparable to a few electron gyroradii. The distributions consist of a core with $T_{\parallel} > T_{\perp}$ and a nongyrotropic crescent perpendicular to the magnetic field. The crescents are associated with finite gyroradius effects of partly demagnetized electrons.

My contribution: I planned the study, performed the data analysis and lead the writing of the paper.

Paper V

Observation of high-shear bifurcated electron-scale current sheet at the magnetopause

Manuscript in preparation.

Studies based on MMS data have already led to many observations related to magnetic reconnection, thin current sheets, and the electron dynamics therein, and have shown that the diversity of current sheet structures is remarkable. In this paper, we expand upon these observation by reporting observations of a thin electron-scale current sheet that has a distinct bifurcated structure. The current sheet has features consistent with guide-field magnetic reconnection close to the electron diffusion region, such as strong out-of-plane currents, Hall electric and magnetic fields, and perpendicular crescent-shaped electron distributions associated with finite gyroradius effects. We find that the crescent distributions carry perpendicular currents with magnitudes comparable to the parallel currents and are thus an integral part of the current system supporting the magnetic field structure. Electrons behave adiabatically in the vicinity of the current sheet where they convect with the magnetic field into the magnetic reconnection inflow region.

My contribution so far: I have planned the study, performed the data analysis and I am leading the writing of the paper.

11. Sammanfattning på svenska

En stor del av det synliga universum består av plasma, en gas där var och en av partiklarna är elektriskt laddad men där den totala laddningen är noll. Exempel är jordens omgivning (över några hundra kilometers höjd), andra planeters omgivningar och stora delar av solen och stjärnorna. Från solens yta blåser en vind med plasma och magnetfält, solvinden. Jorden har ett magnetfält som sträcker sig ut i rymden och som träffas av solvinden. Magnetfältet skapar en bubbla med låg plasmatäthet runt jorden, magnetosfären. Stora volymer av rymden består av relativt homogent plasma som rör sig tillsammans med magnetfältet, till exempel i solvinden samt i stora delar av planetära magnetosfärer. Dessa stora volymer är ofta separerade från varandra längs tunna utsträcka gränsskikt. Många småskaliga processer i dessa gränsskikt förmedlar stora mängder plasma och energi mellan de olika regionerna och kan leda till globala ändringar i magnetfältstopologin. För att förstå hur stora nästan homogena regioner skapas, upprätthålls samt blandas är det således viktigt att förstå hur processer i de tunna skikten fungerar.

Vi studerar vad som händer i tunna gränsområden mellan två stora plasmaområden med magnetfält, till exempel där solvinden träffar jordens magnetfält. Partiklarna i de stora områdena följer det magnetiska fältet, man säger att partiklarna är "infrusna". Om magnetfältet i de två plasmaområdena har olika riktning kan man tro att partiklarna från de två områdena aldrig kan blandas. Men områdena kommer att skiljas av ett tunt skikt med strömmar. Processer i detta tunna skikt gör att partiklarna kan blandas och få tillgång till energi som finns lagrad i de motriktade magnetfälten. Det är processer i denna typ av tunna skikt vi vill förstå, processer som sedan påverkar mycket stora volymer i rymden. Rymden runt jorden ovanför jonosfären är väsentligen kollisionsfri, detta betyder att informations-, energi- och massöverföring måste ske genom andra medel. Detta sker genom växelverkan mellan elektromagnetiska fält och de laddade partiklar som utgör ett plasma. Instabiliteter som skapar elektromagnetiska vågor kan således spela en viktig roll i energiöverföringen mellan fält och partiklar, samt olika partikelpopulationer, till exempel mellan elektroner och joner.

En viktig process i tunna strömskikt kallas ”magnetisk omkoppling” (på engelska ”magnetic reconnection”). Denna process resulterar i storskaliga ändringar i magnetfältstopologin och överför energi från magnetfältet till partiklar. Processen är viktig för att solvinden ska kunna tränga in i jordens magnetosfär, där energin kan ge upphov till bland annat norrsken. Processen orsakar också att stora bubblor med plasma kan skjutas ut från solytan och orsaka

störningar i rymdvädret runt jorden. Magnetisk omkoppling är också viktig inom astrofysiken och inom laboratorie- och fusionsforskning. Magnetisk omkoppling är en flerskalig process som involverar både joner och elektroner. Flera fundamentala delar av processen är ännu inte förklarade. Några viktiga frågor att besvara är hur processen startar, vilken roll elektroner spelar på de minsta längdskalorna, samt hur energin som överförs till plasmat fördelas.

För att studera plasmaprocesser i tunna skikt, inklusive magnetisk omkoppling, använder vi observationer från ESA's fyra Cluster-satelliter uppsända år 2000 i formationsflygning runt jorden. På varje satellit finns instrument för att mäta elektriska och magnetiska fält, samt laddade partiklar. Vi använder också data från NASA's fyra MMS-satelliter uppsända i formationsflygning 2015. Dessa farkoster har motsvarande typer av instrument ombord. Det specifika målet med MMS är att studera magnetisk omkoppling. Vi studerar småskaliga – skalan där detaljer kring elektronernas rörelse blir viktig– processer i tunna gränsskikt. I magnetosfären runt jorden innebär detta ofta längdskalor på några kilometer. Vi har bland annat gjort noggranna mätningar av både vågrörelser i elektromagnetiska fält och av elektrostatiska solitära strukturer, två mekanismer som båda kan koppla samman elektroner och joner i ett plasma utan kollisioner. Detta kan bland annat orsaka resistans, alltså inbromsning av elektroner som bär en ström. Specifikt har vi studerat så kallade lägre-hybrid vågor samt elektrostatiska solitära strukturer i form av så kallade elektronhål i plasmat.

Vi har även karaktäriserat elektroners dynamik i tunna strömskikt och funnit att strömmen ofta bärs av elektroner vars bana är komplicerad på grund av starka gradienter i magnetfältet. Strömmar i tunna skikt är av fundamental betydelse för hur magnetisk omkoppling startar och fungerar.

Processer på de små skalor vi studerar i tunna strömskikt har tidigare på grund av instrumentella begränsningar aldrig kunnat studeras i rymden. Resultaten kommer att leda till bättre förståelse av vår närmiljö i rymden, men även av grundläggande plasmafysik.

References

[1] Miah M. Adel. A detector telescope's pitch angle sampling of magnetospheric particles. *Earth, Planets and Space*, 60(7):753–761, 2008.

[2] H. Alfvén. Existence of Electromagnetic-Hydrodynamic Waves. *Nature*, 150:405–406, October 1942.

[3] M. J. Aschwanden. *Physics of the Solar Corona. An Introduction with Problems and Solutions (2nd edition)*. Springer-Verlag Berlin Heidelberg, December 2005.

[4] S. D. Bale, F. S. Mozer, and T. Phan. Observation of lower hybrid drift instability in the diffusion region at a reconnecting magnetopause. *Geophys. Res. Lett.*, 29(24):2180, December 2002.

[5] W. Baumjohann and R. A. Treumann. *Basic space plasma physics*. Imperial College Press, London, 1997.

[6] J. Berchem and C. T. Russell. The thickness of the magnetopause current layer - ISEE 1 and 2 observations. *Journal of Geophysical Research*, 87:2108–2114, April 1982.

[7] N. Bessho, L.-J. Chen, J. R. Shuster, and S. Wang. Electron distribution functions in the electron diffusion region of magnetic reconnection: Physics behind the fine structures. *Geophys. Res. Lett.*, 41:8688–8695, December 2014.

[8] D. Biskamp. *Magnetic Reconnection in Plasmas*, volume 3 of *Cambridge monographs on plasma physics*. Cambridge University Press, September 2000.

[9] Pål. Brekke and Fredrik Broms. *Northern lights - a guide*. Press, 2013.

[10] O. Buneman. Dissipation of Currents in Ionized Media. *Physical Review*, 115:503–517, August 1959.

[11] J. L. Burch, T. E. Moore, R. B. Torbert, and B. L. Giles. Magnetospheric Multiscale Overview and Science Objectives. *Space Science Reviews*, May 2015.

[12] J. L. Burch and T. D. Phan. Magnetic reconnection at the dayside magnetopause: Advances with MMS. *Geophys. Res. Lett.*, 43:8327–8338, August 2016.

[13] J. L. Burch, R. B. Torbert, T. D. Phan, L.-J. Chen, T. E. Moore, R. E. Ergun, J. P. Eastwood, D. J. Gershman, P. A. Cassak, M. R. Argall, S. Wang, M. Hesse, C. J. Pollock, B. L. Giles, R. Nakamura, B. H. Mauk, S. A. Fuselier, C. T. Russell, R. J. Strangeway, J. F. Drake, M. A. Shay, Yu. V. Khotyaintsev, P.-A. Lindqvist, G. Marklund, F. D. Wilder, D. T. Young, K. Torkar, J. Goldstein, J. C. Dorelli, L. A. Avanov, M. Oka, D. N. Baker, A. N. Jaynes, K. A. Goodrich, I. J. Cohen, D. L. Turner, J. F. Fennell, J. B. Blake, J. Clemmons, M. Goldman, D. Newman, S. M. Petrinec, K. J. Trattner, B. Lavraud, P. H. Reiff, W. Baumjohann, W. Magnes, M. Steller, W. Lewis, Y. Saito, V. Coffey, and M. Chandler. Electron-scale measurements of magnetic reconnection in space. *Science*, 2016.

[14] I. H. Cairns and B. F. McMillan. Electron acceleration by lower hybrid waves in magnetic reconnection regions. *Physics of Plasmas*, 12(10):102110–+, October 2005.
[15] R. C. Carrington. Description of a Singular Appearance seen in the Sun on September 1, 1859. , 20:13–15, November 1859.
[16] T. A. Carter, H. Ji Yamada, R. M Kulsrud, and F. Trintchouk. Experimental study of lower-hybrid drift turbulence in reconnecting current sheet. *Physics of Plasmas*, 9(8), 2002.
[17] P. A. Cassak, D. J. Mullan, and M. A. Shay. From Solar and Stellar Flares to Coronal Heating: Theory and Observations of How Magnetic Reconnection Regulates Coronal Conditions. *The Astrophysical Journal*, 676:L69, March 2008.
[18] P. A. Cassak and M. A. Shay. Scaling of asymmetric magnetic reconnection: General theory and collisional simulations. *Physics of Plasmas*, 14(10):102114, October 2007.
[19] C. A. Cattell, J. Dombeck, J. R. Wygant, M. K. Hudson, F. S. Mozer, M. A. Temerin, W. K. Peterson, C. A. Kletzing, C. T. Russell, and R. F. Pfaff. Comparisons of Polar satellite observations of solitary wave velocities in the plasma sheet boundary and the high altitude cusp to those in the auroral zone. *Geophys. Res. Lett.*, 26:425–428, February 1999.
[20] H. Che, J. F. Drake, M. Swisdak, and M. L. Goldstein. The adiabatic phase mixing and heating of electrons in Buneman turbulence. *Physics of Plasmas*, 20(6):061205, June 2013.
[21] H. Che, J. F. Drake, M. Swisdak, and P. H. Yoon. Electron holes and heating in the reconnection dissipation region. *Geophys. Res. Lett.*, 37:11105, June 2010.
[22] F. F. Chen. *Plasma Physics and Controlled Fusion*. Springer, 2 edition, 2006.
[23] Li-Jen Chen, Michael Hesse, Shan Wang, Naoki Bessho, and William Daughton. Electron energization and structure of the diffusion region during asymmetric reconnection. *Geophysical Research Letters*, pages n/a–n/a, 2016. 2016GL068243.
[24] A. J. Coates, F. J. Crary, G. R. Lewis, D. T. Young, J. H. Waite, and E. C. Sittler. Discovery of heavy negative ions in Titan's ionosphere. *Geophys. Res. Lett.*, 34:22103, November 2007.
[25] J. W. S. Cook, S. C. Chapman, R. O. Dendy, and C. S. Brady. Self-consistent kinetic simulations of lower hybrid drift instability resulting in electron current driven by fusion products in tokamak plasmas. *Plasma Physics and Controlled Fusion*, 53(6):065006–+, June 2011.
[26] William Crookes. On radiant matter. A lecture delivered to the British Association for the Advancement of Science, 1879.
[27] F. Darrouzet, J. de Keyser, and V. Pierrard. *The Earth's Plasmasphere*. Springer, 2009.
[28] F. Darrouzet, V. Pierrard, S. Benck, G. Lointier, J. Cabrera, K. Borremans, N. Y. Ganushkina, and J. D. Keyser. Links between the plasmapause and the radiation belt boundaries as observed by the instruments CIS, RAPID, and WHISPER onboard Cluster. *Journal of Geophysical Research (Space Physics)*, 118:4176–4188, July 2013.
[29] W. Daughton. Electromagnetic properties of the lower-hybrid drift instability

in a thin current sheet. *Physics of Plasmas*, 10:3103–3119, August 2003.
[30] W. Daughton, G. Lapenta, and P. Ricci. Nonlinear Evolution of the Lower-Hybrid Drift Instability in a Current Sheet. *Physical Review Letters*, 93(10):105004–+, September 2004.
[31] R. C. Davidson and N. T. Gladd. Anomalous transport properties associated with the lower-hybrid-drift instability. *Physics of Fluids*, 18:1327–1335, October 1975.
[32] A. Divin, Y. V. Khotyaintsev, A. Vaivads, and M. André. Lower hybrid drift instability at a dipolarization front. *Journal of Geophysical Research (Space Physics)*, 120:1124–1132, February 2015.
[33] G. A. Doschek, D. E. McKenzie, and H. P. Warren. Plasma Dynamics Above Solar Flare Soft X-Ray Loop Tops. *The Astrophysical Journal*, 788:26, June 2014.
[34] J. F. Drake, M. Opher, M. Swisdak, and J. N. Chamoun. A Magnetic Reconnection Mechanism for the Generation of Anomalous Cosmic Rays. *The Astrophysical Journal*, 709:963–974, February 2010.
[35] J. F. Drake, M. Swisdak, C. Cattell, M. A. Shay, B. N. Rogers, and A. Zeiler. Formation of Electron Holes and Particle Energization During Magnetic Reconnection. *Science*, 299:873–877, February 2003.
[36] J. P. Eastwood, T. D. Phan, M. Øieroset, and M. A. Shay. Average properties of the magnetic reconnection ion diffusion region in the Earth's magnetotail: The 2001-2005 Cluster observations and comparison with simulations. *Journal of Geophysical Research (Space Physics)*, 115:8215, August 2010.
[37] S. Eriksson, B. Lavraud, F. D. Wilder, J. E. Stawarz, B. L. Giles, J. L. Burch, W. Baumjohann, R. E. Ergun, P.-A. Lindqvist, W. Magnes, C. J. Pollock, C. T. Russell, Y. Saito, R. J. Strangeway, R. B. Torbert, D. J. Gershman, Y. V. Khotyaintsev, J. C. Dorelli, S. J. Schwartz, L. Avanov, E. Grimes, Y. Vernisse, A. P. Sturner, T. D. Phan, G. T. Marklund, T. E. Moore, W. R. Paterson, and K. A. Goodrich. Magnetospheric Multiscale observations of magnetic reconnection associated with Kelvin-Helmholtz waves. *Geophys. Res. Lett.*, 43:5606–5615, June 2016.
[38] C. P. Escoubet, M. Fehringer, and M. Goldstein. IntroductionThe Cluster mission. *Annales Geophysicae*, 19:1197–1200, 2001.
[39] G. Federici, C. H. Skinner, J. N. Brooks, J. P. Coad, C. Grisolia, A. A. Haasz, A. Hassanein, V. Philipps, C. S. Pitcher, J. Roth, W. R. Wampler, and D. G. Whyte. REVIEW: Plasma-material interactions in current tokamaks and their implications for next step fusion reactors. *Nuclear Fusion*, 41:1967–2137, December 2001.
[40] W. Fox, M. Porkolab, J. Egedal, N. Katz, and A. Le. Laboratory Observation of Electron Phase-Space Holes during Magnetic Reconnection. *Physical Review Letters*, 101(25):255003, December 2008.
[41] B. D. Fried and S. D. Conte. *The Plasma Dispersion Function*. Academic Press, New York NY, 1961.
[42] S. A. Fuselier, W. S. Lewis, C. Schiff, R. Ergun, J. L. Burch, S. M. Petrinec, and K. J. Trattner. Magnetospheric Multiscale Science Mission Profile and Operations. *Space Science Reviews*, 199:77–103, March 2016.
[43] W. Gekelman, H. Pfister, Z. Lucky, J. Bamber, D. Leneman, and J. Maggs.

Design, construction, and properties of the large plasma research device - The LAPD at UCLA. *Review of Scientific Instruments*, 62:2875–2883, December 1991.
[44] William Gilbert. *On the magnet, magnetick bodies also, and on the great magnet the earth*. 1600.
[45] S. Gillmar and J. R. Spreiter, editors. *Discovery of the magnetosphere*. American Geophysical Union, 2013.
[46] R. G. Giovanelli. A Theory of Chromospheric Flares. , 158:81–82, July 1946.
[47] J. Goodman and D. Uzdensky. Reconnection in Marginally Collisionless Accretion Disk Coronae. , 688:555–558, November 2008.
[48] D. B. Graham, Y. V. Khotyaintsev, A. Vaivads, and M. André. Electrostatic solitary waves and electrostatic waves at the magnetopause. *Journal of Geophysical Research (Space Physics)*, 121:3069–3092, April 2016.
[49] D. B. Graham, Yu. V. Khotyaintsev, C. Norgren, A. Vaivads, M. André, P.-A. Lindqvist, G. T. Marklund, R. E. Ergun, W. R. Paterson, D. J. Gershman, B. L. Giles, C. J. Pollock, J. C. Dorelli, L. A. Avanov, B. Lavraud, Y. Saito, W. Magnes, C. T. Russell, R. J. Strangeway, R. B. Torbert, and J. L. Burch. Electron currents and heating in the ion diffusion region of asymmetric reconnection. *Geophysical Research Letters*, pages n/a–n/a, 2016. 2016GL068613.
[50] D. A. Gurnett and A. Bhattacharjee. *Introduction to Plasma Physics*. Cambridge University Press, January 2005.
[51] L. N. Hans. *Analytical Mechanics*. Cambridge University Press, 2008.
[52] M. Hesse, N. Aunai, D. Sibeck, and J. Birn. On the electron diffusion region in planar, asymmetric, systems. *Geophys. Res. Lett.*, 41:8673–8680, December 2014.
[53] M. Hesse and J. Birn. On the cessation of magnetic reconnection. *Annales Geophysicae*, 22:603–612, February 2004.
[54] M. Hesse, Y.-H. Liu, L.-J. Chen, N. Bessho, M. Kuznetsova, J. Birn, and J. L. Burch. On the electron diffusion region in asymmetric reconnection with a guide magnetic field. *Geophys. Res. Lett.*, 43:2359–2364, March 2016.
[55] M. Hesse, K. Schindler, J. Birn, and M. Kuznetsova. The diffusion region in collisionless magnetic reconnection. *Physics of Plasmas*, 6:1781–1795, May 1999.
[56] F. L. Hinton and R. D. Hazeltine. Theory of plasma transport in toroidal confinement systems. *Reviews of Modern Physics*, 48:239–308, April 1976.
[57] R. Hodgson. On a curious Appearance seen in the Sun. , 20:15–16, November 1859.
[58] M. Horányi, T. W. Hartquist, O. Havnes, D. A. Mendis, and G. E. Morfill. Dusty plasma effects in Saturn's magnetosphere. *Reviews of Geophysics*, 42:4002, December 2004.
[59] J. D. Huba, N. T. Gladd, and K. Papadopoulos. The lower-hybrid-drift instability as a source of anomalous resistivity for magnetic field line reconnection. , 4:125–126, 1977.
[60] J. D. Huba, N. T. Gladd, and K. Papadopoulos. Lower-hybrid-drift wave turbulence in the distant magnetotail. , 83:5217–5226, November 1978.
[61] M. E. Innocenti, C. Norgren, D. Newman, M. Goldman, S. Markidis, and

G. Lapenta. Study of electric and magnetic field fluctuations from lower hybrid drift instability waves in the terrestrial magnetotail with the fully kinetic, semi-implicit, adaptive multi level multi domain method. *Physics of Plasmas*, 23(5):052902, May 2016.

[62] ITER Physics Basis Editors, ITER Physics Expert Group Chairs, ITER Joint Central Team, and Physics Integration Unit. Chapter 1: Overview and summary. *Nuclear Fusion*, 39:2137–2174, December 1999.

[63] J. Jara-Almonte, W. Daughton, and H. Ji. Debye scale turbulence within the electron diffusion layer during magnetic reconnection. *Physics of Plasmas*, 21(3):032114, March 2014.

[64] Jonathan Jara-Almonte, Hantao Ji, Masaaki Yamada, Jongsoo Yoo, and William Fox. Laboratory observation of resistive electron tearing in a two-fluid reconnecting current sheet. *Phys. Rev. Lett.*, 117:095001, Aug 2016.

[65] Bence Jones. *The life and letters of Faraday*. London, Longmans, Green and Co., 1870.

[66] H. Karimabadi, V. Roytershteyn, H. X. Vu, Y. A. Omelchenko, J. Scudder, W. Daughton, A. Dimmock, K. Nykyri, M. Wan, D. Sibeck, M. Tatineni, A. Majumdar, B. Loring, and B. Geveci. The link between shocks, turbulence, and magnetic reconnection in collisionless plasmas. *Physics of Plasmas*, 21(6):062308, June 2014.

[67] Y. V. Khotyaintsev, A. Vaivads, M. André, M. Fujimoto, A. Retinò, and C. J. Owen. Observations of Slow Electron Holes at a Magnetic Reconnection Site. *Physical Review Letters*, 105(16):165002, October 2010.

[68] Yu. V. Khotyaintsev, D. B. Graham, C. Norgren, E. Eriksson, W. Li, A. Johlander, A. Vaivads, M. André, P. L. Pritchett, A. Retino, T. D. Phan, R. E. Ergun, K. Goodrich, P.-A. Lindqvist, G. T. Marklund, O. Le Contel, F. Plaschke, W. Magnes, R. J. Strangeway, C. T. Russell, H. Vaith, M. R. Argall, C. A. Kletzing, R. Nakamura, R. B. Torbert, W. R. Paterson, D. J. Gershman, J. C. Dorelli, L. A. Avanov, B. Lavraud, Y. Saito, B. L. Giles, C. J. Pollock, D. L. Turner, J. D. Blake, J. F. Fennell, A. Jaynes, B. H. Mauk, and J. L. Burch. Electron jet of asymmetric reconnection. *Geophysical Research Letters*, pages n/a–n/a, 2016. 2016GL069064.

[69] Kristian Kirkeland. *The norwegian aurora polaris expedition 1902-1903*. Christiania H. Aschehoug and co., 1908.

[70] M. G. Kivelson and C. T. Russel, editors. *Introduction to Space Physics*. Cambridge University Press, 1995.

[71] N. A. Krall and P. C. Liewer. Low-frequency instabilities in magnetic pulses. *Phys. Rev. A*, 4:2094–2103, Nov 1971.

[72] I. Langmuir. Oscillations in Ionized Gases. *Proceedings of the National Academy of Science*, 14:627–637, August 1928.

[73] G. Lapenta, J. U. Brackbill, and W. S. Daughton. The unexpected role of the lower hybrid drift instability in magnetic reconnection in three dimensions. *Physics of Plasmas*, 10:1577–1587, May 2003.

[74] G. Lapenta, S. Markidis, A. Divin, M. V. Goldman, and D. L. Newman. Bipolar electric field signatures of reconnection separatrices for a hydrogen plasma at realistic guide fields. , 38:17104, September 2011.

[75] B. Lavraud, Y. C. Zhang, Y. Vernisse, D. J. Gershman, J. Dorelli, P. A. Cassak,

J. Dargent, C. Pollock, B. Giles, N. Aunai, M. Argall, L. Avanov, A. Barrie, J. Burch, M. Chandler, L.-J. Chen, G. Clark, I. Cohen, V. Coffey, J. P. Eastwood, J. Egedal, S. Eriksson, R. Ergun, C. J. Farrugia, S. A. Fuselier, V. Génot, D. Graham, E. Grigorenko, H. Hasegawa, C. Jacquey, I. Kacem, Y. Khotyaintsev, E. MacDonald, W. Magnes, A. Marchaudon, B. Mauk, T. E. Moore, T. Mukai, R. Nakamura, W. Paterson, E. Penou, T. D. Phan, A. Rager, A. Retino, Z. J. Rong, C. T. Russell, Y. Saito, J.-A. Sauvaud, S. J. Schwartz, C. Shen, S. Smith, R. Strangeway, S. Toledo-Redondo, R. Torbert, D. L. Turner, S. Wang, and S. Yokota. Currents and associated electron scattering and bouncing near the diffusion region at Earth's magnetopause. *Geophysical Research Letters*, pages n/a–n/a, 2016. 2016GL068359.

[76] B. Lefebvre, L.-J. Chen, W. Gekelman, P. Kintner, J. Pickett, P. Pribyl, and S. Vincena. Debye-scale solitary structures measured in a beam-plasma laboratory experiment. *Nonlinear Processes in Geophysics*, 18:41–47, January 2011.

[77] B. Lefebvre, L.-J. Chen, W. Gekelman, P. Kintner, J. Pickett, P. Pribyl, S. Vincena, F. Chiang, and J. Judy. Laboratory Measurements of Electrostatic Solitary Structures Generated by Beam Injection. *Physical Review Letters*, 105(11):115001, September 2010.

[78] D. M. Malaspina, D. L. Newman, L. B. Wilson, III, K. Goetz, P. J. Kellogg, and K. Kersten. Electrostatic Solitary Waves in the Solar Wind: Evidence for Instability at Solar Wind Current Sheets. *Journal of Geophysical Research (Space Physics)*, 118:591–599, February 2013.

[79] H. Matsumoto, H. Kojima, T. Miyatake, Y. Omura, M. Okada, I. Nagano, and M. Tsutsui. Electrotastic Solitary Waves (ESW) in the magnetotail: BEN wave forms observed by GEOTAIL. *Geophys. Res. Lett.*, 21:2915–2918, December 1994.

[80] J. Clerk Maxwell. A dynamical theory of the electromagnetic field. *Philosophical Transactions of the Royal Society of London*, 155:459–512, 1865.

[81] F. S. Mozer, V. Angelopoulos, J. Bonnell, K. H. Glassmeier, and J. P. McFadden. THEMIS observations of modified Hall fields in asymmetric magnetic field reconnection. *Geophys. Res. Lett.*, 35:L17S04, April 2008.

[82] Yasuhito Narita. *Plasma Turbulence in the Solar System*. Springer, 2012.

[83] C. Norgren, D. B. Graham, Yu. V. Khotyaintsev, M. André, A. Vaivads, L.-J. Chen, P.-A. Lindqvist, G. T. Marklund, R. E. Ergun, W. Magnes, R. J. Strangeway, C. T. Russell, R. B. Torbert, W. R. Paterson, D. J. Gershman, J. C. Dorelli, L. A. Avanov, B. Lavraud, Y. Saito, B. L. Giles, C. J. Pollock, and J. L. Burch. Finite gyroradius effects in the electron outflow of asymmetric magnetic reconnection. *Geophysical Research Letters*, pages n/a–n/a, 2016. 2016GL069205.

[84] K. Papadopoulos. A review of anomalous resistivity for the ionosphere. *Reviews of Geophysics and Space Physics*, 15:113–127, February 1977.

[85] E. N. Parker. Newtonian development of the dynamical properties of ionized gases of low density. *Phys. Rev.*, 107:924–933, Aug 1957.

[86] E. N. Parker. Sweet's Mechanism for Merging Magnetic Fields in Conducting Fluids. *Journal of Geophysical Research*, 62:509–520, December 1957.

[87] A. L. Peratt. Advances in Numerical Modeling of Astrophysical and Space Plasmas. *Astrophysics and Space Science*, 242:93–163, March 1996.

[88] H. E. Petschek. Magnetic Field Annihilation. *NASA Special Publication*, 50:425, 1964.

[89] J. S. Pickett, L.-J. Chen, R. L. Mutel, I. W. Christopher, O. Santolik, G. S. Lakhina, S. V. Singh, R. V. Reddy, D. A. Gurnett, B. T. Tsurutani, E. Lucek, and B. Lavraud. Furthering our understanding of electrostatic solitary waves through Cluster multispacecraft observations and theory. *Advances in Space Research*, 41:1666–1676, 2008.

[90] E. Priest and T. Forbes. *Magnetic Reconnection*. Cambridge University Press, 2000.

[91] P. L. Pritchett. Onset and saturation of guide-field magnetic reconnection. *Physics of Plasmas*, 12(6):062301, June 2005.

[92] P. L. Pritchett. Collisionless magnetic reconnection in an asymmetric current sheet. *Journal of Geophysical Research (Space Physics)*, 113:6210, June 2008.

[93] Z.-Y. Pu, K. B. Quest, M. G. Kivelson, and C.-Y. Tu. Lower-hybrid-drift instability and its associated anomalous resistivity in the neutral sheet of earth's magnetotail. *Journal of Geophysical Research*, 86:8919–8928, October 1981.

[94] A. Retinò, M. B. Bavassano Cattaneo, M. F. Marcucci, A. Vaivads, M. André, Y. Khotyaintsev, T. Phan, G. Pallocchia, H. Rème, E. Möbius, B. Klecker, C. W. Carlson, M. McCarthy, A. Korth, R. Lundin, and A. Balogh. Cluster multispacecraft observations at the high-latitude duskside magnetopause: implications for continuous and component magnetic reconnection. *Annales Geophysicae*, 23:461–473, February 2005.

[95] J. G. Roederer. Earth's magnetosphere: Global problems in Magnetospheric Plasma Physics. In *Space Plasma Physics: The Study of Solar-System Plasmas. Volume 2, working papers. Part I – Solar-system Magnetohydrodynamics*. the National Academy of Sciences, 1979.

[96] Ingrid Sandahl. *Norrsken: Budbärare från Rymden*. Atlantis, 1998.

[97] B. U. O. Sonnerup, G. Paschmann, I. Papamastorakis, N. Sckopke, G. Haerendel, S. J. Bame, J. R. Asbridge, J. T. Gosling, and C. T. Russell. Evidence for magnetic field reconnection at the earth's magnetopause. , 86:10049–10067, November 1981.

[98] B. U.O. Sonnerup. Magnetic Field Reconnection. In *Space Plasma Physics: The Study of Solar-System Plasmas. Volume 2, working papers. Part II – Solar System Plasma Processes*. the National Academy of Sciences, 1979.

[99] T. H. Stix. *Waves in plasmas*. 1992.

[100] D. G. Swanson. *Plasma waves*. Academic Press, 1989.

[101] P. A. Sweet. The Neutral Point Theory of Solar Flares. In B. Lehnert, editor, *Electromagnetic Phenomena in Cosmical Physics*, volume 6 of *IAU Symposium*, page 123, 1958.

[102] K. G. Tanaka, A. Retinò, Y. Asano, M. Fujimoto, I. Shinohara, A. Vaivads, Y. Khotyaintsev, M. André, M. B. Bavassano-Cattaneo, S. C. Buchert, and C. J. Owen. Effects on magnetic reconnection of a density asymmetry across the current sheet. *Annales Geophysicae*, 26:2471–2483, August 2008.

[103] J. B. Tao, R. E. Ergun, L. Andersson, J. W. Bonnell, A. Roux, O. LeContel,

V. Angelopoulos, J. P. McFadden, D. E. Larson, C. M. Cully, H.-U. Auster, K.-H. Glassmeier, W. Baumjohann, D. L. Newman, and M. V. Goldman. A model of electromagnetic electron phase-space holes and its application. *Journal of Geophysical Research (Space Physics)*, 116:11213, November 2011.

[104] K. J. Trattner, J. S. Mulcock, S. M. Petrinec, and S. A. Fuselier. Location of the reconnection line at the magnetopause during southward IMF conditions. *Geophys. Res. Lett.*, 34:L03108, February 2007.

[105] L. Trenchi, M. F. Marcucci, G. Pallocchia, G. Consolini, M. B. Bavassano Cattaneo, A. M. di Lellis, H. RèMe, L. Kistler, C. M. Carr, and J. B. Cao. Occurrence of reconnection jets at the dayside magnetopause: Double Star observations. *Journal of Geophysical Research (Space Physics)*, 113:A07S10, July 2008.

[106] R. A. Treumann. Origin of resistivity in reconnection. *Earth, Planets, and Space*, 53:453–462, June 2001.

[107] Rudolf Treumann and Wolfgang Baumjohann. Collisionless magnetic reconnection in space plasmas. *Frontiers in Physics*, 1:31, 2013.

[108] A. Vaivads, M. André, S. C. Buchert, J.-E. Wahlund, A. N. Fazakerley, and N. Cornilleau-Wehrlin. Cluster observations of lower hybrid turbulence within thin layers at the magnetopause. , 31:L03804, February 2004.

[109] A. Vaivads, Y. Khotyaintsev, M. André, and R. A. Treumann. Plasma Waves Near Reconnection Sites. In J. W. Labelle and R. A. Treumann, editors, *Geospace Electromagnetic Waves and Radiation*, volume 687 of *Lecture Notes in Physics, Berlin Springer Verlag*, page 251, January 2006.

[110] A. Vaivads, A. Retinò, and M. André. Magnetic reconnection in space plasma. *Plasma Physics and Controlled Fusion*, 51(12):124016–+, December 2009.

[111] J. A. van Allen and L. A. Frank. Radiation Around the Earth to a Radial Distance of 107,400 km. , 183:430–434, February 1959.

[112] H. Viberg, Y. V. Khotyaintsev, A. Vaivads, M. André, and J. S. Pickett. Mapping HF waves in the reconnection diffusion region. , 40:1032–1037, March 2013.

[113] M. Yamada, H. Ji, S. Hsu, T. Carter, R. Kulsrud, N. Bretz, F. Jobes, Y. Ono, and F. Perkins. Study of driven magnetic reconnection in a laboratory plasma. *Physics of Plasmas*, 4:1936–1944, May 1997.

[114] J. Yoo, M. Yamada, H. Ji, J. Jara-Almonte, C. E. Myers, and L.-J. Chen. Laboratory Study of Magnetic Reconnection with a Density Asymmetry across the Current Sheet. *Physical Review Letters*, 113(9):095002, August 2014.

[115] P. H. Yoon and A. T. Y. Lui. Drift instabilities in current sheets with guide field. *Physics of Plasmas*, 15(7):072101–+, July 2008.

Acta Universitatis Upsaliensis

Digital Comprehensive Summaries of Uppsala Dissertations from the Faculty of Science and Technology 1453

Editor: The Dean of the Faculty of Science and Technology

A doctoral dissertation from the Faculty of Science and Technology, Uppsala University, is usually a summary of a number of papers. A few copies of the complete dissertation are kept at major Swedish research libraries, while the summary alone is distributed internationally through the series Digital Comprehensive Summaries of Uppsala Dissertations from the Faculty of Science and Technology. (Prior to January, 2005, the series was published under the title "Comprehensive Summaries of Uppsala Dissertations from the Faculty of Science and Technology".)

Distribution: publications.uu.se
urn:nbn:se:uu:diva-307955

ACTA
UNIVERSITATIS
UPSALIENSIS
UPPSALA
2016